Article

Solution and Film Self-Assembly Behavior of a Block Copolymer Composed of a Poly(ionic Liquid) and a Stimuli-Responsive Weak Polyelectrolyte

Kayla Foley and Keisha B. Walters*

Read Online

ACCESS | Metrics & More | Article Recommendations | SI Supporting Information

ABSTRACT: Cu(0)-mediated atom transfer radical polymerization was used to synthesize a poly(ionic liquid), poly[4-vinylbenzyl-3-butylimidazolium bis(trifluoromethylsulfonyl)imide] (PVBBImTf$_2$N), a stimuli-responsive polyelectrolyte, poly[2-(dimethylamino)ethyl methacrylate] (PDMAEMA), and a novel block copolymer formed from these two polymers. The synthesis of the block copolymer, poly[2-(dimethylamino) ethyl methacrylate]-*block*-[poly(4-vinylbenzyl-3-butylimidazolium bis-(trifluoromethylsulfonyl)imide] (PDMAEMA-*b*-PVBBImTf$_2$N), was examined to evaluate the control of "livingness" polymerization, as indicated by molecular weight, characterizations of degree of polymerization, and ^{1}HNMR spectroscopy. 2D DOSY

NMR measurements revealed the successful formation of block copolymer and the connection between the two polymer blocks. PDMAEMA-*b*-PVBBImTf$_2$N was further characterized for supramolecular interactions in both the bulk and solution states through FTIR and ^{1}H NMR spectroscopies. While the block copolymer demonstrated similar intermolecular behavior to the PIL homopolymer in the bulk state as indicated by FTIR, hydrogen bonding and counterion interactions in solution were observed in polar organic solvent through ^{1}H NMR measurements. The DLS characterization revealed that the PDMAEMA-*b*-PVBBImTf$_2$N block copolymer forms a network-like aggregated structure due to a combination of hydrogen bonding between the PDMAEMA and PIL group and electrostatic repulsive interactions between PIL blocks. This structure was found to collapse upon the addition of KNO$_3$ while still maintaining hydrogen bonding interactions. AFM-IR analysis demonstrated varied morphologies, with spherical PDMAEMA in PVBBImTf$_2$N matrix morphology exhibited in the region approaching the film center. AFM-IR further revealed signals from silica nano-contaminates, which selectively interacted with the PDMAEMA spheres, demonstrating the potential for the PDMAEMA-*b*-PVBBImTf$_2$N PIL block copolymer in polymer−inorganic nanoparticle composite applications.
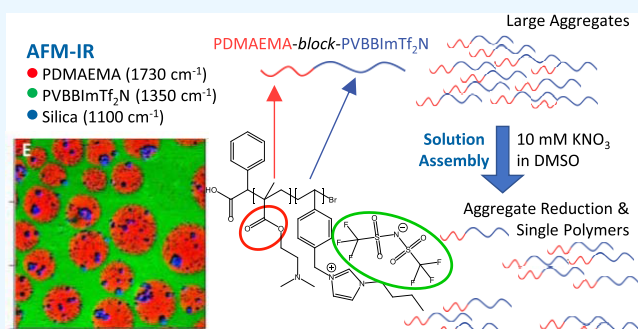
■ INTRODUCTION

Poly(ionic liquids) (PILs) are a special type of strong polyelectrolytes that combine the diverse functionality and unique properties of ionic liquids (ILs) with the mechanical stability, long-range ordering, and processability of polymers.[1−3] In recent years, PILs have emerged as innovative functional polyelectrolytes with applications in a variety of fields, including battery electrolytes, separations, nanomaterials, and more.[4−10] In the past decade, PILs have been combined with highly incompatible neutral polymers to form block copolymers (BCPs) either in solution or as films. These systems have been used in forming polymer films and membranes with unique nanostructures such as lamellae, cylinders, spheroids, and bicontinuous structures.[9,11−13] In solution, they can form various structures (e.g., micellar spheres, vesicles, cubosomes) that are modulated by salt environment and PIL design[14−19] in addition to traditional BCP assembly behaviors (e.g., solvent, polymer block length, concentration).[20] Depending on the structure, these morphol-

ogies and supramolecular interactions can enhance the properties of PILs materials, such as ion conductivity in battery electrolytes[9,11,21,22] or interfacial behavior in emulsions.[23]

While neutral-poly(ionic liquid) block copolymers have been explored in some depth, there are only a few reports of all-PIL block copolymers[23−26] and of PILs blocked with weak polyelectrolytes.[19,27,28] All-polyelectrolyte PILs block copolymers are of potential interest as they enable an increase in the overall charge density and ion conductivity, thereby improving overall electrochemical properties and providing multiple blocks that are both tunable by simple ion exchange. Thus
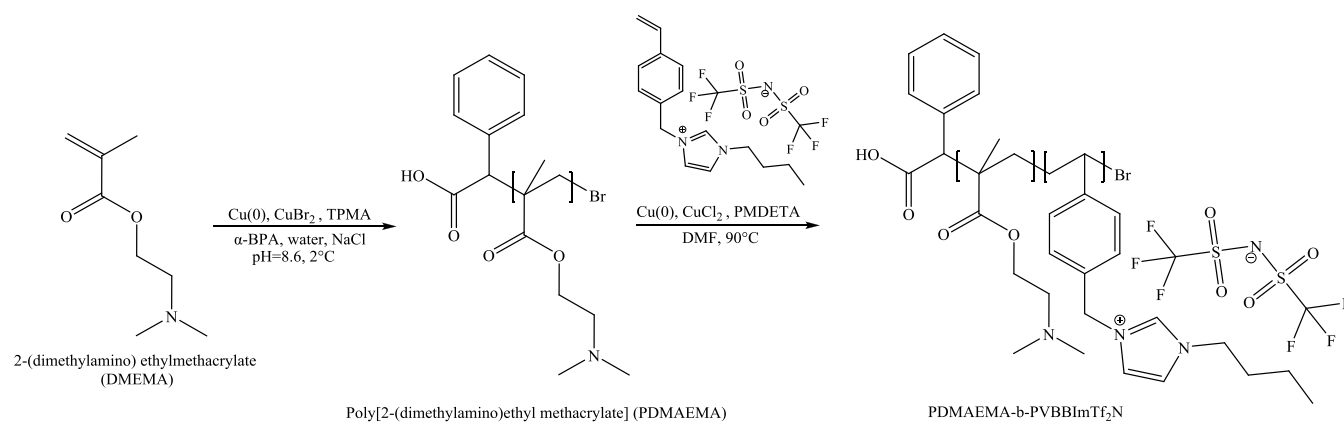
Figure 1. Schematic illustration of the Cu(0)-mediated ATRP process showing first the synthesis of the PDMAEMA macroinitiator using DMAEMA in pH 8.6 aqueous conditions. The PDMAEMA block was then used as a macroinitiator to polymerize the PVBBImTf₂N PIL block in dimethylformamide (DMF), resulting in the PDMAEMA-*b*-PVBBImTf₂N block copolymer.

far, the all-PIL block copolymers systems examined mainly consisted of polyvinylimidazolium-based PIL blocks where covalent alterations to the imidazolium pendant alkyl chain or the spacer chain between the polymer backbone and imidazolium group are the main drivers for self-assembly behavior in solution.[23−26] Further, the self-assembled structures produced in these systems have been generally limited to spherical or rodlike micelles in solution.[24,26] Additionally, to the authors' knowledge, no study has examined the self-assembly behavior of all-PIL block copolymers in the bulk or as films.

Blocking PILs with weak polyelectrolytes instead offers additional design parameters for controlling self-assembly behavior including the ability to modulate the charge density based on the degree of protonation. Such materials show conformational changes in response to environmental stimuli such as changes in pH and salt.[29,30] The weak polyelectrolyte block may also be used to control the overall charge density of the block copolymer, which can aid in controlled solid electrolyte design or polyelectrolyte gels. However, only a few studies have investigated block copolymers composed of PILs and weak polyelectrolytes—either anionic[16,19,31] or cationic[28]—and of these, only the solution self-assembly behavior has been examined. Synthesizing and characterizing novel PIL-b-polyelectrolytes and expanding studies to include bulk phase self-assembly characterization of polyelectrolyte block copolymers will aid in the development of novel all-polyelectrolyte materials for stimuli response, polymer battery electrolyte, and flexible electronics applications.[1,10,32]

In this work, a novel cationic (PIL-*b*-polyelectrolyte) BCP was synthesized through Cu(0)-mediated atom transfer radical polymerization (ATRP), a type of controlled "living" radical polymerization technique. Specifically, poly[4-vinylbenzyl-3-butylimidazolium bis(trifluoromethylsulfonyl) imide] (PVBBImTf₂N) was polymerized utilizing a tertiary amine, weak polyelectrolyte macroinitiator to prepare the block copolymer poly[2-(dimethylamino) ethyl methacrylate]-*block*-poly[4-vinylbenzyl-3-butylimidazolium bis-(trifluoromethylsulfonyl)imide] block copolymer (PDMAEMA-*b*-PVBBImTf₂N). The synthesized polymers were characterized for their molecular weight and polymerization "livingness" using a combination of gel permeation chromatography (GPC) and nuclear magnetic resonance (NMR). The chemical structure and supramolecular behavior as a bulk polymer and

in solution were also investigated using NMR and Fourier transform infrared (FTIR) spectroscopies, indicating a combination of hydrogen bonding and electrostatic interactions occurring in the block copolymer. In addition, dynamic light scattering (DLS) was employed in a polar organic solvent to investigate the solubility and solution behavior of the block copolymer in response to added salt. It was noteworthy to mention that the block copolymer demonstrated an extended hierarchical aggregate structure in pure polar organic solvent, which resulted in a collapse in aggregate sizes upon addition of salt. Furthermore, self-assembly of the unique poly(ionic liquid)-*block*-(poly)tertiary amine with the stimuli-responsive weak polyelectrolyte block was further examined using solution-cast films and, for the first time in a PIL system, via simultaneous infrared-atomic force microscopy (AFM-IR). In brief, this paper focuses on the synthesis of a novel all-poly(ionic liquid) diblock copolymer as well as an initial examination of its solution self-assembly behavior in response to added salt and film assembly behavior through a unique AFM-IR technique.

■ RESULTS AND DISCUSSION

Cu(0)-mediated ATRP is a controlled polymerization technique that uses a zero-valence metal to *in situ* produce the Cu(I) activating species through comproportionation, which then mediates the monomer addition to the polymer chain backbone in a controlled manner.[33−35] ATRP is characterized by pseudo-first-order kinetics as determined by a linear $\ln[M]_o/[M]$ plot with time, where M_o and M are the monomer concentration initially and at time, t, respectively. ATRP also allows for predicting the degree of polymerization (DP) and the number-average molecular weight (M_n) based on the starting monomer (M_o) and initiator (I_o) concentrations and conversion (χ) and monomer molecular weight $(\mathrm{MW}_{monomer})$:

$$\mathrm{DP}^{\mathrm{theo}} = \frac{[M]_o}{[I]_o}\chi$$

$$M_n^{\mathrm{theo}} = \mathrm{DP}(\mathrm{MW}_{monomer})$$

This method generally produces narrow polydispersity indices (ratio of weight-average molecular weight, M_w, to number-average molecular weight, M_n, PDI = M_w/M_n) of less than ≤1.5 for polyelectrolytes.[19,36]
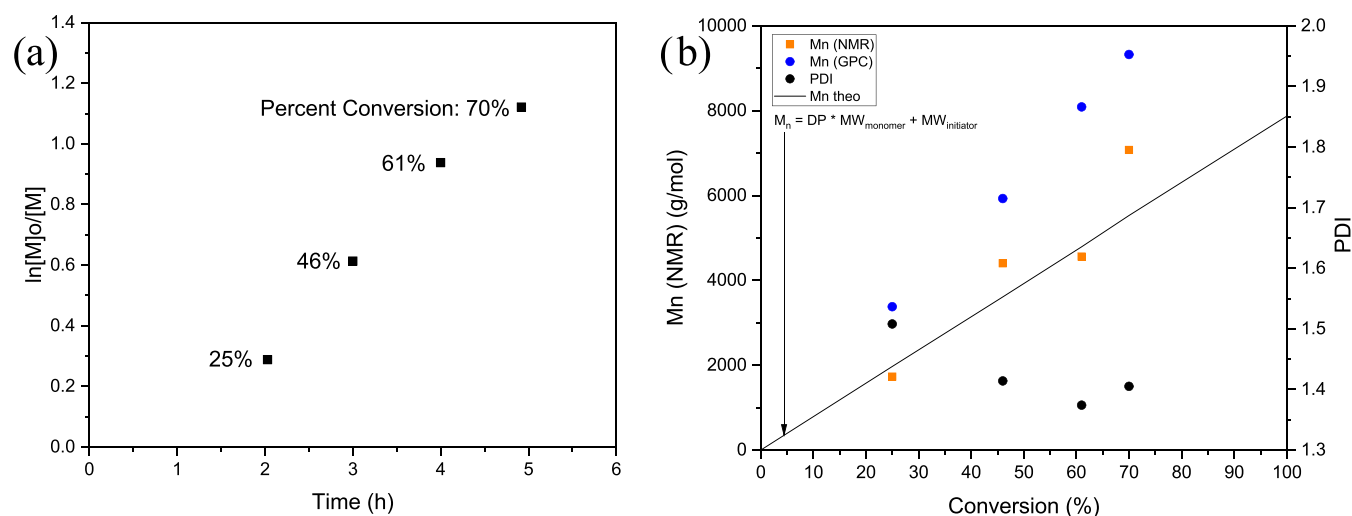
Figure 2. PDMAEMA shows (a) pseudo-first-order kinetics through a linear $\ln[M]_o/[M]$ response with time. (b) Relatively narrow PDIs of $\sim$1.5 were observed for the macroinitiator (black circles). M_n increased linearly with time with slightly higher values observed for the GPC results (blue circles) (9,323 g/mol at 70% conversion) compared to the NMR (orange circles) (7,074 g/mol at 70% conversion) calculated values. Both M_n values were slightly higher than the theoretical M_n (5,531 g/mol) calculated based on initial monomer and initiator concentrations ($[M]_o/[I]_o = 50$).

Here, the block copolymer poly[(2-(dimethylamino)ethyl methacrylate)]-*block*-poly[4-vinylbenzyl-3-butylimidazolium bis(trifluoromethylsulfonyl)imide] (PDMAEMA-*b*-PVBBImTf$_2$N) was synthesized using PDMAEMA as a macroinitiator to form an all-polyelectrolyte PIL block copolymer (Figure 1). PDMAEMA was selected as it has a weak tertiary amine pendant group that can be protonated at pH values lower than $\sim$7.5 (pK_a $\sim$7 to 8) to form cationic charge groups.[34,37,38] Further, PDMAEMA has been previously found to display material property changes in response to pH and salt.[39,40] An imidazolium-based PIL with a styrenic polymer backbone was selected as it has been successfully polymerized by ATRP methods previously.[12,41−43] Additionally, the styrenic backbone will provide hydrophobic content to facilitate microphase separation behavior between the two blocks.

Polymerization of the Tertiary Amine Macroinitiator PDMAEMA. The macroinitiator was synthesized using an aqueous-based Cu(0)-mediated ATRP procedure recently reported by the authors' group.[34] Figure 2 shows the kinetic results for the macroinitiator synthesis in aqueous solution. The PDMAEMA displayed pseudo-first-order kinetics as demonstrated by the linear increase in $\ln[M]_o/[M]$ with time (Figure 2a) with a final monomer conversion of $\sim$70%. The final polymer had a degree of polymerization (DP$_{PDMAEMA,NMR}$) and number-average molecular weight ($M_n^{PDMAEMA,NMR}$) of 45 units and 7,074 g/mol, respectively, as calculated by NMR peak integral ratioing (Figure 2b). Aqueous gel permeation chromatography (GPC) results using PEG standards gave a slightly higher molecular weight and degree of polymerization ($M_n^{PDMAEMA,GPC}$ = 9,323 g/mol and DP$_{PDMAEMA,GPC}$ = 59 units) with a moderate polydispersity of 1.41, which is comparable to other ATRP synthesis studies of PDMAEMA in the literature.[44,45] The difference between the NMR- and GPC-determined molecular weights may stem from the moderate 1.41 polydispersity as well as from several factors in the GPC measurement process such as polymer−column interactions and the difference between the hydrodynamic volume behavior of the PEG calibration standards and the

PDMAEMA.[46,47] The NMR-calculated $M_n^{PDMAEMA,NMR}$ and DP$_{PDMAEMA,NMR}$ for the PDMAEMA macroinitiator will be used for comparisons with the PIL block copolymer.

Block Copolymerization of PDMAEMA-b-PVBBImTf$_2$N and Comparison to PVBBImTf$_2$N Homopolymerization. Figure 3 shows the kinetic results for the PVBBImTf$_2$N homopolymer and the PDMAEMA-*b*-PVBBImTf$_2$N block copolymer. Due to solubility issues and column interactions, GPC measurements were not possible for the PIL-based polymers, even with the addition of 10 mM LiTf$_2$N salt to the mobile phase to reduce column interactions following the method used successfully by Matyjaszewski et al.[14] Other light scattering methods for determining molecular weight were also not possible due to the poor solubility. Instead, NMR peak integral ratioing was used to determine monomer conversion and polymer DP$_{PVBBImTf2N,NMR}$ as has been done by other groups with similar issues.[48−50] It is noted that the actual degree of polymerization for the block copolymer determined in comparison to this macroinitiator may vary due to the moderate polydispersity of the PDMAEMA macroinitiator and that the values reported here are an estimate based on the NMR ratio analysis between the two polymer blocks.

The PVBBImTf$_2$N homopolymerization showed a linear increase in $\ln[M]_o/[M]$ (Figure 3a) and conversion (Figure 3b) as a function of time. Since the polymer conversion proceeds up to 76% at 24 h, the PVBBImTf$_2$N homopolymerization reaction appears to be controlled. Therefore, the slight deviation at the 8 h time point for the homopolymer may be due to sampling or measurement error. The $\ln[M]_o/[M]$ and conversion versus time data suggest pseudo-first-order kinetics, and this result matches prior literature reports of controlled ATRP PVBBImTf$_2$N homopolymerizations.[43,51] The PDMAEMA-*b*-PVBBImTf$_2$N block copolymer (chain extension) polymerization showed a steeper increase in conversion (from 0 to 58%) in 1 h than the homopolymerization, followed by a gradual increase to 67% conversion at 24 h (Figure 3b). The $\ln[M]_o/[M]$ plot shows a similar sharp increase followed by a plateau between 1 and 24 h. The rapid increase in conversion and $\ln[M]_o/[M]$ during the first hour of

(a)

(b)

(c)
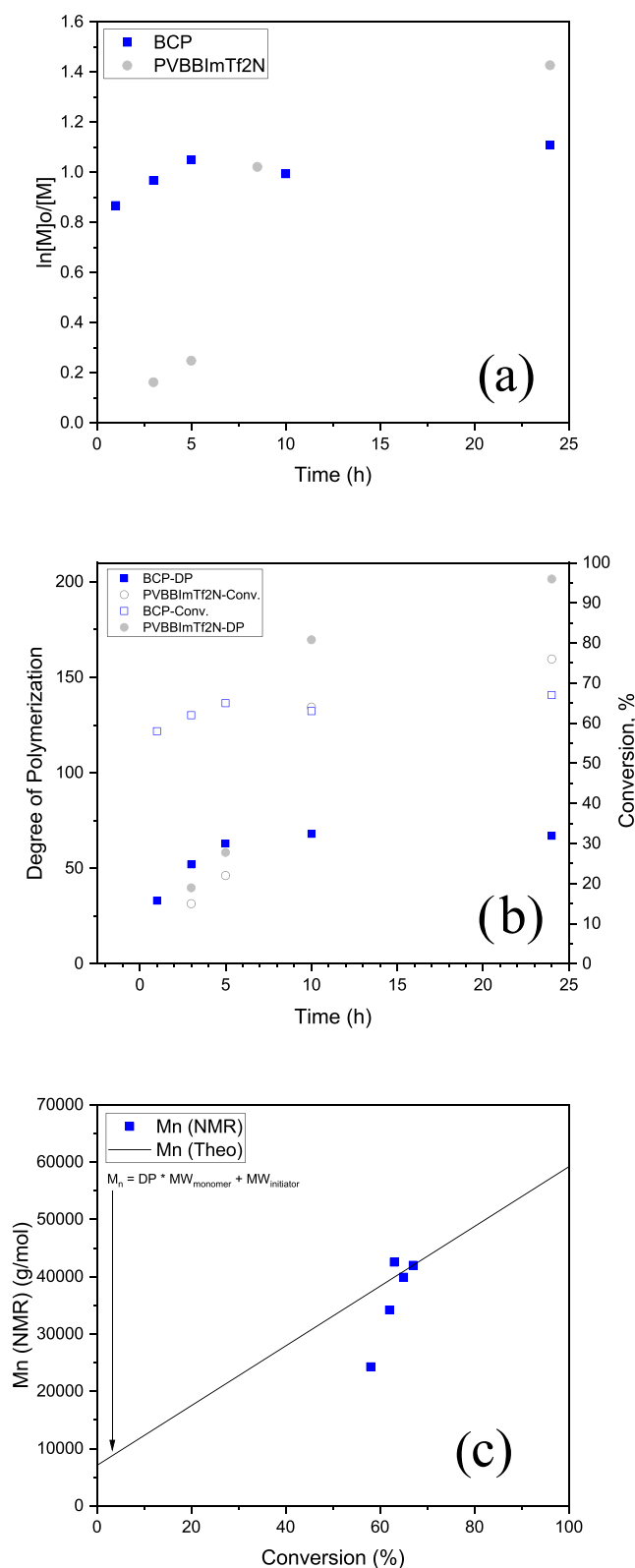
Figure 3. (a) Pseudo-first-order kinetics are observed for the PVBBImTf$_2$N homopolymer (gray circles) but not necessarily for the PDMAEMA-*b*-PVBBImTf$_2$N block copolymer (blue circles). (b) Conversion increased linearly with time for the PVBBImTf$_2$N homopolymer (gray open circles) to 76% (at 24 h). The block copolymer (blue open squares) increased sharply in the first hour to 58% conversion before gradually increasing to 67% conversion after 24 h. PDMAEMA-*b*-PVBBImTf$_2$N DP$_{PVBBImTf2N,NMR}$ (blue filled squares) increased gradually from ∼33 units (1 h) to ∼63 units in

Figure 3. continued

the first 5 h before increasing slightly to 67 units (24 h) at the end of the reaction while the homopolymer PVBBImTf$_2$N degree of polymerization increased linearly with time (gray filled circles). (c) NMR-calculated M_n (42,014 g/mol) corresponds closely to the theoretical M_n (42,011 g/mol for $[M]_o/[I]_o = 100$) at 67% conversion after 24 h.

the PVBBImTf$_2$N block polymerization for the PDMAEMA-*b*-PVBBImTf$_2$N copolymer indicates a faster kinetics for this chain extension reaction than was observed for the PVBBImTf$_2$N homopolymerization. These faster kinetics were not expected and so time points were not collected in the first hour of the reaction; therefore, controlled polymerization for PDMAEMA-*b*-PVBBImTf$_2$N cannot be confirmed. The plateau observed for the chain extension to form the block copolymer longer than 10 h may be due to chain termination.[43,51,52]

DP$_{PVBBImTf2N, NMR}$ was determined using NMR by ratioing the benzyl group peak integral in the PVBBImTf$_2$N block to the tertiary amine methyl group peak integral in the PDMAEMA block and assuming a 45-unit DP$_{PDMAEMA, NMR}$ for the PDMAEMA block. Here, the block copolymer showed a linear increase in DP$_{PVBBImTf2N,NMR}$ from ∼33 units at 1 h to 63 units at 5 h before plateauing to ∼67 units at 24 h, similarly suggesting controlled polymerization in the first 5 h of the reaction before chain termination reactions take over. The degree of polymerization for the PVBBImTf$_2$N block is close to the theoretically predicted DP$_{PVBBImTf2N,Theo}$ (67 units) and $M_n^{PVBBImTf2N,Theo}$ (42,011 g/mol) for 67% conversion for $[M]_o/[I]_o = 100$ as calculated by

$$DP = \left(\frac{[M]_o}{[I]_o} \chi \right)$$

and

$$M_n = \left(\frac{[M]_o}{[I]_o} \times conversion \right) MW_{monomer} + M_n^{PDMAEMA}$$

where $M_n^{PDMAEMA,NMR}$ (7,074 g/mol) is the number-average molecular weight of the PDMAEMA block with a 45-unit DP$_{PDMAEMA,NMR}$. Overall, the block copolymer by NMR peak integral ratioing was estimated to have a 45-unit PDMAEMA block, 67-unit PVBBImTf$_2$N block, and an overall $M_n^{PDMAEMA-b-PVBBImTf2N}$ of ∼42 kDa, although a broader molecular weight distribution is likely due to the indicated chain termination reactions longer than 10 h. The estimated degree of polymerization of the PIL block matches well with the theoretically predicted DP and overall molecular weight despite the uncaptured data in the 1st hour of the block copolymer polymerization. In order to confirm the successful polymerization and connectivity of the polymer blocks, FTIR and NMR spectroscopies were performed for the PDMAEMA MI, PVBBImTf$_2$N homopolymer, and PDMAEMA-*b*-PVBBImTf$_2$N block copolymer. These spectroscopic studies also provided insight into supramolecular bonding interactions occurring in the bulk polymer and in solution conditions.

Chemical Structure and Bonding. Figure 4a,b shows the ATR-FTIR spectra for the polymers and VBBImTf$_2$N monomer above 2200 cm^{-1} and below 1800 cm^{-1}, respectively. In the VBBImTf$_2$N monomer, PVBBImTf$_2$N homopolymer, and PDMAEMA-*b*-PVBBImTf$_2$N block copoly-
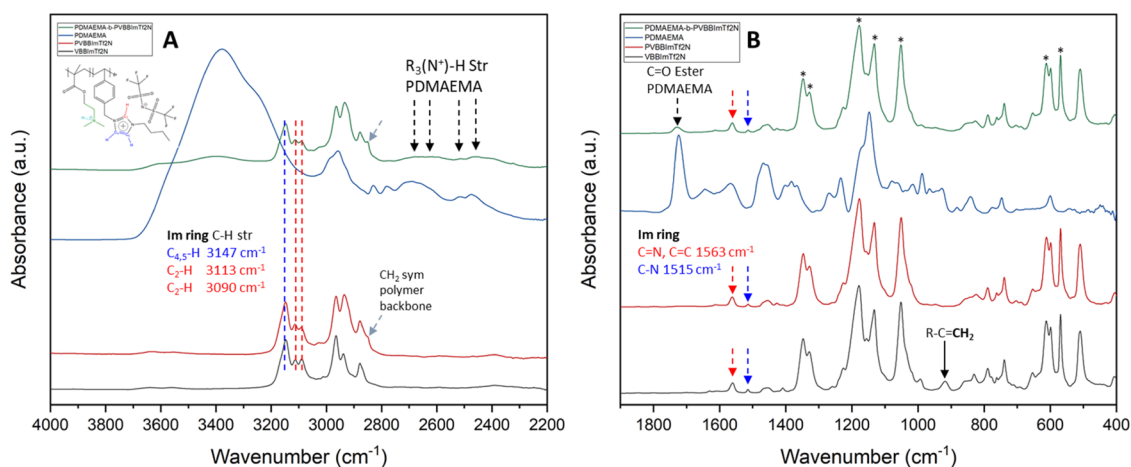
Figure 4. ATR-FTIR results for the VBBImTf$_2$N monomer (black), PVBBImTf$_2$N homopolymer (red), PDMAEMA macroinitiator (blue), and PDMAEMA-*b*-PVBBImTf$_2$N block copolymer in the (A) 4000−2200 cm^{-1} and (B) <1800 cm^{-1} regions. Red and blue arrows and dotted lines indicate the C$_2$-H and C$_{4,5}$-H imidazolium ring methylene stretches, respectively. Gray arrows mark the 2850 cm^{-1} peak corresponding to CH$_2$ sym str of the polymer backbone. Black dotted arrows mark the N$^+$-H str and combinations modes of the protonated tertiary amine group and the ester C═O str in the PDMAEMA block. The solid black arrow indicates the vinyl group in the VBBImTf$_2$N IL monomer, and the black asterisks designate the Tf$_2$N$^-$ anion modes.
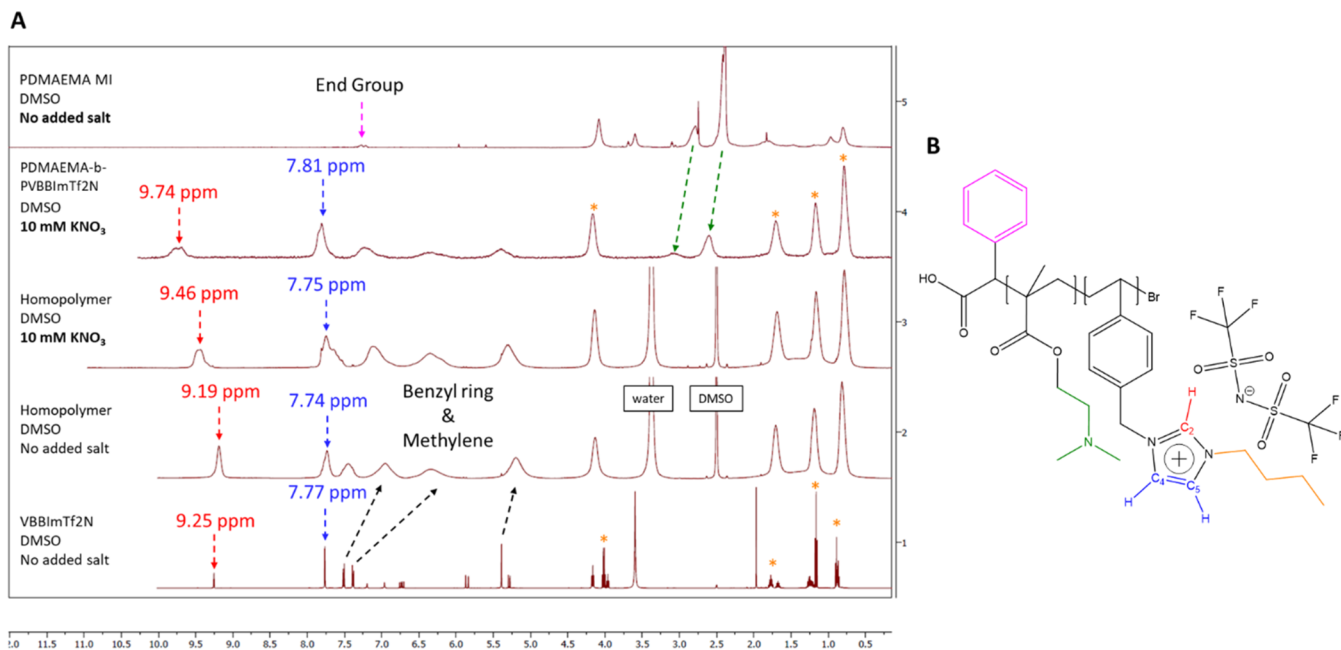
Figure 5. (A) NMR results (bottom to top) for the VBBImTf$_2$N monomer in DMSO-d_6, PVBBImTf$_2$N homopolymer in DMSO-d_6, PVBBImTf$_2$N homopolymer in 10 mM KNO$_3$ DMSO-d_6 solution, PDMAEMA-*b*-PVBBImTf$_2$N block copolymer in 10 mM KNO$_3$ DMSO-d_6 solution, and PDMAEMA macroinitiator in DMSO-d_6. Orange asterisks mark the imidazolium butyl chain CH$_2$/CH$_3$ protons. Green arrows mark the shift in the PDMAEMA tertiary amine and methylene groups. Red and blue arrows mark the shifts in the C$_2$-H and C$_{4,5}$-H protons, respectively, and (B) correspond to the colored portions of the PDMAEMA-*b*-PVBBImTf$_2$N chemical structure.

mer samples, the peaks at 3147, 3113, and 3090 cm^{-1} are assigned to the C$_2$ and C$_{4,5}$ C−H stretches on the imidazolium ring. The first peak is typically attributed to the C$_{4,5}$-H stretches of the diene group, and the latter two peaks are typically attributed to the more acidic C$_2$-H proton.[53,54] These imidazolium ring protons are sensitive to hydrogen bonding and intermolecular interactions and may show shifts in absorbances depending on the counterion type and other intermolecular interactions.[55−57] In this case, both the PIL homopolymer and the block copolymer have similar absorbances for the C$_2$-H and C$_{4,5}$-H protons as the

VBBImTf$_2$N monomer, indicating a similar intermolecular environment of the imidazolium ring for both the dry homo- and block copolymers. The emergence of a peak at 2850 cm^{-1} in the PVBBImTf$_2$N and PDMAEMA-*b*-PVBBImTf$_2$N samples is typically for the symmetrical CH$_2$ stretching modes of the polymer backbone.[58,59] Several peaks in the 3000−2870 cm^{-1} region are due to various asymmetrical and symmetrical CH$_2$/CH$_3$ stretching modes from the methylene groups and alkyl chains present in both polymers.[58,60] Several weak N$^+$-H stretch and combination modes in the 2800−2400 cm^{-1} region were also observed in the PDMAEMA-*b*-PVBBImTf$_2$N and
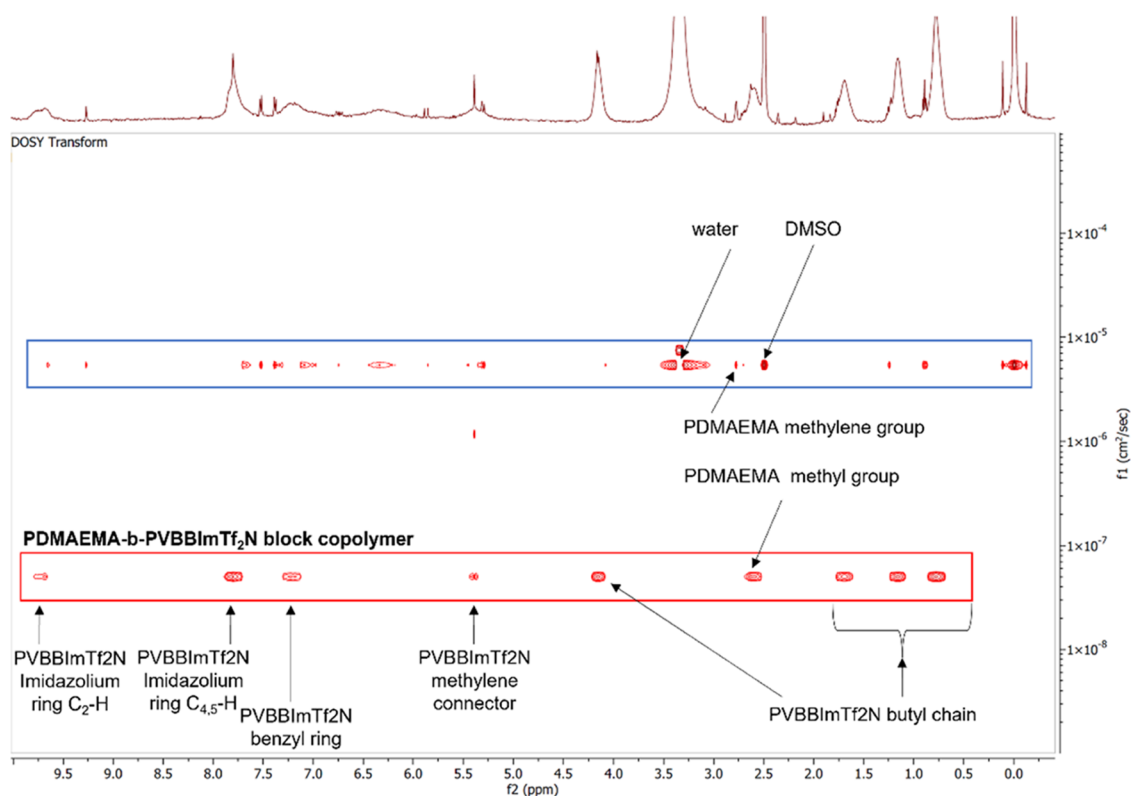
Figure 6. NMR 2D DOSY showing the diffusion-separated PDMAEMA-*b*-PVBBImTf$_2$N proton signals (red box) with a lower diffusion coefficient at ~10^{-8} cm^2/s compared to the residual VBBImTf$_2$N monomer, PDMAEMA MI, water, and DMSO signals (blue box) at 10^{-6} cm^2/s.

PDMAEMA samples.[61] These peaks are typical for tertiary amine salts, which indicates at least partial protonation of the tertiary amine group in the block copolymer after synthesis. As the PDMAEMA was synthesized in pH ~ 8.6 conditions, the protonation likely results from a drop in pH to below the pK_a of PDMAEMA (pK_a ~ 7 to 8)[34,38] during the purification step on precipitation with ammonium sulfate.[62]

Below 1800 cm^{-1}, the C=O ester stretch at ~1728 cm^{-1} from the PDMAEMA block is observed in the block copolymer sample[63] (Figure 4b). A loss of the 920 cm^{-1} vinyl bending mode (R-C=CH$_2$) in the PVBBImTf$_2$N homopolymer and block copolymer further confirms polymerization and successful purification of the polymers.[58,60] Also characteristic of the PIL are the imidazolium ring C=N/C=C stretches at 1563 cm^{-1} and the C−N stretch at 1515 cm^{-1} for the PVBBImTf$_2$N block,[54,64,65] which are also at similar wavenumbers in both the homo- and block copolymer PILs. This suggests the cation−anion interaction environment does not change on block copolymerization with PDMAEMA when in the bulk polymer state. Several intense peaks for the Tf$_2$N$^-$ anion were also observed at 1346 cm^{-1} (SO$_2$ asym str), 1330 cm^{-1} (SO$_2$ asym str), 1178 cm^{-1} (SO$_2$ sym str), 1133 cm^{-1} (SO$_2$ sym str), 1050 cm^{-1} (C-S str), 612 cm^{-1} (SNS bending), and 569 cm^{-1} (CF$_3$ bending), which compare well to the literature.[54,55,64,66]

FTIR results confirm the successful polymerization of the block copolymer through the loss of the monomer vinyl group IR modes. The spectra also indicate partial protonation of the PDMAEMA block and similar cation−anion interaction behavior in the PVBBImT$_2$N block as was also observed for the homopolymer PIL. NMR spectroscopy was performed to corroborate the successful polymerization of the PDMAEMA-

b-PVBBImTf$_2$N block copolymer. In addition to confirming the chemical composition and connectivity of the polymer blocks, the NMR data provides insight into the supramolecular interactions (e.g., cation−anion electrostatic interactions, hydrogen bonding interactions) of the block copolymer in solution and subsequently a better understanding of the solution self-assembly behavior of PDMAEMA-*b*-PVBBImTf$_2$N.

NMR spectra were collected for the VBBImTf$_2$N monomer, PVBBImTf$_2$N homopolymer, PDMAEMA macroinitiator, and PDMAEMA-*b*-PVBBImTf$_2$N block copolymer samples in DMSO-d_6 solvent (Figure 5). Due to solubility issues, it was necessary to add 10 mM KNO$_3$ salt to the PDMAEMA-*b*-PVBBImTf$_2$N solution to improve block copolymer solubility in DMSO and allow for NMR characterization. KNO$_3$ was selected as it has better solubility in DMSO versus other salts such as NaCl and KCl.[67] The block copolymer shows the tertiary amine methyl groups and methylene group peaks at 2.60 and 3.07 ppm, respectively. These are slightly upshifted from 2.38 and 2.78 ppm in PDMAEMA macroinitiator. The benzyl ring (7.23 and 6.32 ppm) and methylene connecting group (5.40 ppm) from the PVBBImTf$_2$N block are present and at approximately the same ppm as the PVBBImTf$_2$N homopolymer. The PVBBImTf$_2$N butyl chain CH$_2$ and CH$_3$ protons are present at ~0.78, 1.17, 1.70, and 4.16 ppm, and these peaks remain relatively constant in the homo- and block copolymer samples. The imidazolium ring C$_2$-H and C$_{4,5}$-H protons were observed in the PIL polymers between 9.75−9.25 and 7.81−7.74 ppm, respectively. A 2D diffusion-ordered (DOSY) NMR experiment (Figure 6; 1D DOSY array provided in the Figure S1) shows the presence of both the PVBBImTf$_2$N and PDMAEMA peaks in the block copolymer
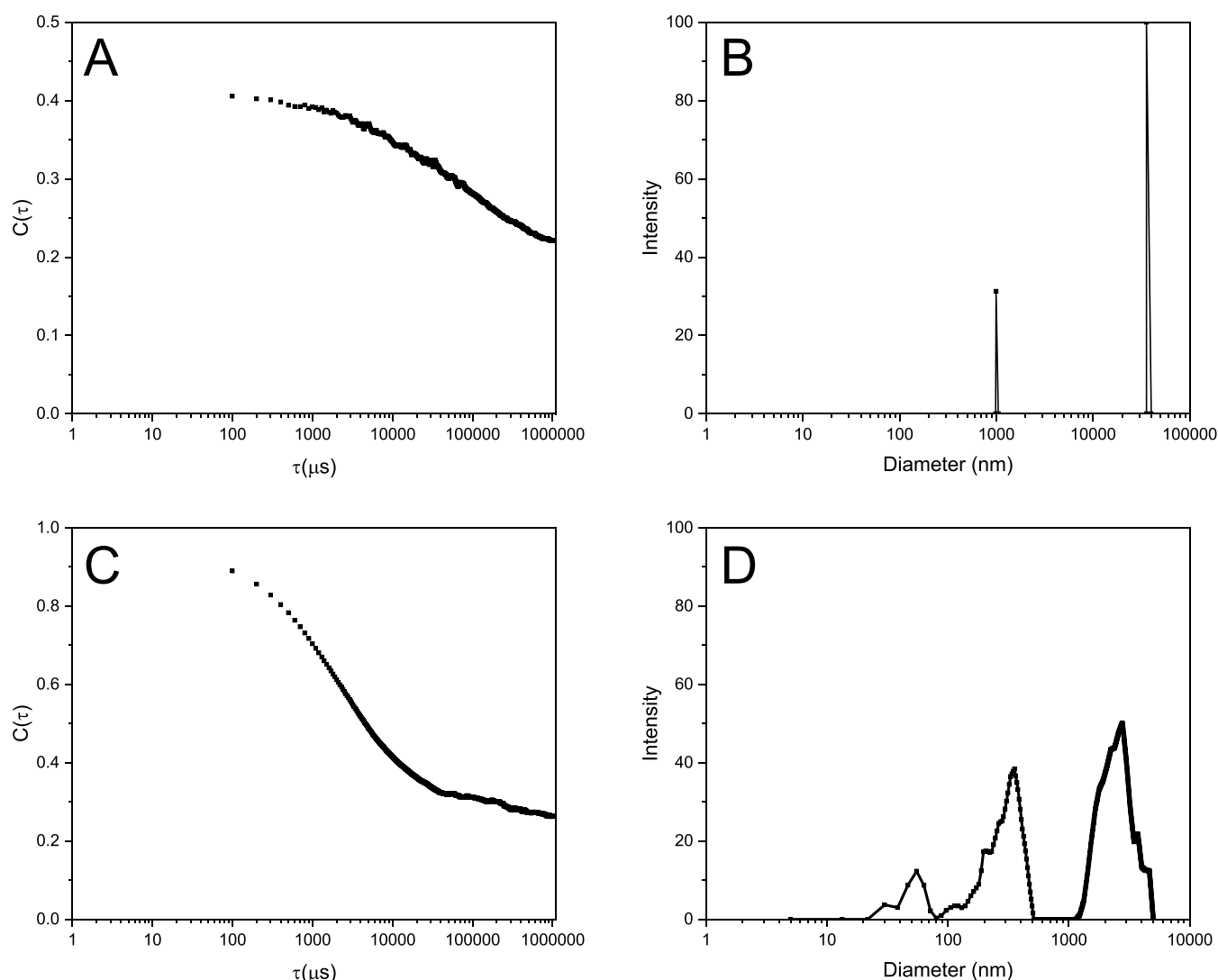
Figure 7. Representative plot of the DLS correlation functions and the corresponding intensity-based hydrodynamic diameters for the PDMAEMA-*b*-PVBBImTf$_2$N block copolymer in (a, b) pure DMSO and (c, d) 10 mM KNO$_3$ DMSO solution, which correspond to the average hydrodynamic diameters provided in Table 1. (b) Particle and aggregate sizes between 500 nm and 54 μm were observed for the block copolymer in pure DMSO. (d) Upon 10 mM KNO$_3$ addition, hydrodynamic diameters decreased by more than an order of magnitude resulting in populations with diameters ranging between 14 and 4,120 nm.

with a diffusion coefficient of 4.9×10^{-8} cm^2/s, confirming successful block copolymerization. Some residual IL monomer and un-chain extended PDMAEMA macroinitiator signals—separate from those for the block copolymer—were also observed with a diffusion coefficient of ~5.4×10^{-6} cm^2/s.

In contrast to the IR results for the bulk polymer, differences in the imidazolium ring proton signals were observed between the PIL homopolymer and block copolymers in solution. The imidazolium ring C$_2$-H and C$_{4,5}$-H protons in the PDMAEMA-*b*-PVBBImTf$_2$N sample are located at 9.74 and 7.81 ppm, respectively. These peaks are upshifted from their signal in the PVBBImTf$_2$N homopolymer (C$_2$-H 9.19 and C$_{4,5}$-H 7.74 ppm) and monomer (C$_2$-H 9.25 and C$_{4,5}$-H 7.77 ppm) with greater shifts observed for the C$_2$-H proton. While all of the protons on the imidazolium ring are capable of hydrogen bonding interactions, the acidic C$_2$-H proton is particularly sensitive to hydrogen bonding interactions between the imidazolium cation and anions in solution.[68] Generally, the strength of hydrogen bonding interactions between C$_2$-H and the counterions increases with decreasing anion size and

increasing coordinating ability of the anion.[69,70] Imidazolium-based PILs containing multiple types of counterions also tend to display intermediate C$_2$-H ppm values between the ppm values observed if only one of the counterions was present.[68,71] However, the PDMAEMA block is also capable of acting as a hydrogen-bond acceptor at the amine nitrogen and carbonyl oxygen, allowing for potential hydrogen bonding interactions with the acidic imidazolium C$_2$-H proton.[72,73] To determine if the C$_2$-H and C$_{4,5}$-H proton peak shifts in the block copolymer were due to partial ion exchange with the added KNO$_3$ salts or due to interactions between polymer blocks, the NMR spectra for the PVBBImTf$_2$N and PDMAEMA homopolymers without and with 10 mM KNO$_3$ salts were also measured.

PVBBImTf$_2$N homopolymer without added salts displays C$_2$-H (9.19 ppm) and C$_{4,5}$-H (7.74 ppm) signals that are slightly shifted downfield in comparison to the VBBImTf$_2$N monomer (C$_2$-H 9.25 and C$_{4,5}$-H 7.77 pm). Horne et al. reported a similar result that was attributed to a weakening of the cation−anion interactions from increased steric effects in the immobilized cation on the polymer backbone or increased

anion dissociation from the PIL imidazolium cation in DMSO.[74] Adding 10 mM KNO$_3$ salt to the PVBBImTf$_2$N homopolymer increases the C$_2$-H signal to 9.46 ppm while the C$_{4,5}$-H signal remains approximately the same (7.75 ppm). The observed 9.46 ppm C$_2$-H peak compares well with other imidazolium-based ILs with nitrate counterions which have been found to have C$_2$-H ppm values between 9.3 and 9.5 ppm in DMSO-d_6 or pure IL.[69,75,76] This increase in the C$_2$-H signal indicates at least partial ion exchange of the NO$_3^-$ anion with the Tf$_2$N$^-$ anion in the PIL homopolymer. These same signals are shifted even further downfield in the PDMAEMA-b-PVBBImTf$_2$N block copolymer with C$_2$-H at 9.74 and C$_{4,5}$-H at 7.81 ppm, indicating the shifts are likely due in part to interactions between the PDMAEMA and PVBBImTf$_2$N blocks in addition to the partial NO$_3^-$ ion exchange. A slight increase in the PDMAEMA tertiary amine methyl and methylene groups in the block copolymer (2.60 and 3.07 ppm) compared to the macroinitiator (2.38 and 2.78 ppm) also support this. Further, no differences in the NMR spectra for the PDMAEMA macroinitiator in pure DMSO-d_6 and 10 mM KNO$_3$ DMSO-d_6 were observed, supporting that the downfield shifts in the macroinitiator methylene and amine methyl groups are due to interactions in between the two polymer blocks and not the salt environment (Supporting Information, Figure S2).

NMR results indicate that the intermolecular environment of the PDMAEMA-b-PVBBImTf$_2$N block copolymer is influenced by both hydrogen bonding interactions between the imidazolium group in the PIL block and the tertiary amine co-block in addition to the salt environment in solution. Such intermolecular interactions can significantly influence the structural behavior of polymers in solution.[77,78] Therefore, to further examine the influence of these supramolecular interactions on the self-assembly behavior of the block copolymer, dynamic light scattering measurements were performed.

Solution Behavior of PDMAEMA-b-PVBBImTf$_2$N Diblock Copolymer. Dynamic light scattering (DLS) measurements were obtained for the PDMAEMA-b-PVBBImTf$_2$N block copolymer in DMSO at 1 mg/mL concentration with and without 10 mM KNO$_3$. While the PDMAEMA-b-PVBBImTf$_2$N block copolymer was found to also swell in other polar organic solvents (Supplemental Table S1), DMSO was selected to allow for a more direct comparison to the NMR results. Figure 7 and Table 1 show the average of eight

Table 1. DLS Summary of the Average Hydrodynamic Diameters for Particle and Aggregate Populations of PDMAEMA-b-PVBBImTf$_2$N in Pure DMSO and 10 mM KNO$_3$ DMSO Solutions[a]

sample	pure DMSO (±std dev)	10 mM KNO$_3$ DMSO (±std dev)
	avg. D_H (nm) by intensity	
population 1		43 ± 13
population 2	995 ± 371	271 ± 91
population 3	35,753 ± 13,257	2,590 ± 761
	avg. D_H (nm) by number	
population 1		57 ± 35
population 2	995 ± 371	

[a]With salt addition, D_H values indicate a mixture of individual polymer strands and aggregates much smaller in size than were observed in DMSO without salt.

measured correlation curves and the hydrodynamic structural lengths for the PDMAEMA-b-PVBBImTf$_2$N block copolymer aggregates in pure DMSO (Figure 7a,b) and DMSO with 10 mM KNO$_3$ salt (Figure 7c,d). Correlation functions and hydrodynamic structural lengths for all eight measurements are also provided in Supplemental Figure S3. For the block copolymer in pure DMSO, the correlation function was best fit by a Dblexp model for bimodal distributions (see Supplemental Figure S4). DLS intensity measurements reveal two populations of large aggregate sizes for the block copolymer in pure DMSO with the smaller population at ∼995 nm (± 371 nm) and a larger population at ∼35.8 μm (±13.3 μm). It should be noted that DLS is typically limited to below ∼10 μm, so while there is indeed a larger aggregate size population observed, the quantitative value of the hydrodynamic diameter should be interpreted with caution. Further, DLS number-based measurements indicate that the ∼995 nm population provides the greatest contribution to the particle size. The addition of KNO$_3$ salt resulted in the collapse of the polymer structure producing three main populations of diameters (by intensity measurements) at ∼43 nm (±13 nm), ∼271 nm (± 91 nm), and 2.6 μm (±0.76 μm), and the resulting correlation function was best fit with an NNLS model (Figure S5). By number-based measurements, a single population with an average particle diameter of 57 nm was observed. This reduction of the overall range of hydrodynamic structural lengths from ∼995 nm to 35.8 μm in pure DMSO to ca. 14 nm to 2.6 μm upon addition of KNO$_3$ indicates that the polyelectrolyte block copolymer structure can be modulated by salt addition as would be expected for polyelectrolyte systems. Generally, increasing the salt content in polyelectrolytes leads to the screening of repulsive interactions between the pendant charge groups on the polymer chain, eventually leading to a collapse from a rodlike structure to a coiled structure similar to the solution behavior of neutral polymers.[79−81]

However, a large portion of the hydrodynamic structural lengths determined by intensity-based measurements in the 10 mM KNO$_3$ DMSO solution are still significantly larger than expected for a solubilized polymer, even upon addition of salt. Based on the NMR analysis, for a block copolymer with estimated degrees of polymerization of ∼45 units (DP$_{PDMAEMA,NMR}$) for the PDMAEMA block and ∼67 units for the PVBBImTf$_2$N block, the fully stretched contour length of a single polymer chain is estimated to be ∼57 nm as calculated by[82]

$$\text{contour length} = \left(2 \text{ atoms}(N_{PDMAEMA} + N_{PVBBImTf2N}) - 1\right)(0.154 \text{ nm})\sin\left(\frac{111.5°}{2}\right)$$

where 0.154 nm is the length of a C-C bond, 111.5° is the bond angle, and $N_{PDMAEMA}$ and $N_{PVBBImTf2N}$ are the number of monomer units for each polymer block. The contour length would be 74 nm if the GPC-determined DP$_{PDMAEMA, GPC}$ of 59 units is assumed instead. The calculated contour length matches well with the smallest intensity-based population (∼43 nm) and the number-based population (∼57 nm), indicating the presence of single solvated polymer chains that are in mostly extended rodlike conformations, as typically observed for charged polyelectrolyte without significant charge screening.[80] However, as several of the populations have hydrodynamic structural lengths significantly larger than these

Figure 8. (a) Hydrogen bonding between the imidazolium C_2-H proton with the PDMAEMA block at the unprotonated tertiary amine and/or the ester carbonyl group. In solution, the PDMAEMA-*b*-PVBBImTf$_2$N copolymer displays (b) in DMSO an extended network structure mediated by hydrogen bonding and repulsive interactions between PIL−PIL blocks and (c) with 10 mM KNO$_3$ salt addition mixture of individual polymer strands and some collapsed aggregate structures. The yellow circles in (b) and (c) indicate hydrogen bonding between PDMAEMA and PVBBImTf$_2$N blocks.

theoretical single-polymer contour lengths, this is indicative of the block copolymer also aggregating into self-assembled hierarchical structures in both pure DMSO and 10 mM KNO$_3$ DMSO. An additional DLS study as a function of KNO$_3$ concentration between 0 and 25 mM also demonstrates a collapse in structure with increasing salt concentration (Supporting Information, Figure S6). The hydrodynamic structural lengths in Figure S6 correspond well to the results as shown in Figure 7.

Based on the NMR and DLS characterization, the proposed solution behavior of the PDMAEMA-*b*-PVBBImTf$_2$N block copolymer in DMSO is depicted in Figure 8. In polar organic solvents, weakly coordinating counterions, such as Tf$_2$N$^-$, are often dissociated from the PIL in solution, resulting in unshielded pendant positive charges on the PIL backbone.[68,74] In the PDMAEMA-*b*-PVBBImTf$_2$N block copolymer system, the dissociation would result in an increased repulsion between the PIL blocks in the polymer chains. As a result, the hydrogen bonding between the imidazolium C_2-H proton and the PDMAEMA block (Figure 8a) likely dominates the block copolymer chain−chain interactions. The combined hydrogen bonding between PDMAEMA/PVBBImTf$_2$N blocks and repulsive interactions between PIL blocks in the block copolymer system results in long strand-like extended networks (Figure 8b). Optical microscopy images of the PDMAEMA-*b*-PVBBImTf$_2$N block copolymer after 24 h in pure DMSO solution revealed long strands and network-like structures, supporting the proposed structure (Supporting Information, Figure S7). Additional images displaying the solvation behavior over time are also provided (Supporting Information, Figures S8−S10).

Upon addition of the KNO$_3$ salt into the solution, the NO$_3^-$ anions more strongly coordinate with the imidazolium ring and help screen some of the positive charges along the PIL block, allowing for PIL−PIL block interactions. While some decrease in hydrogen bonding may occur, as evidenced by NMR characterization of PDMAEMA-*b*-PVBBImTf$_2$N in 10 mM KNO$_3$ DMSO solution, the hydrogen bonding interactions are largely maintained after salt addition. In this case, the reduction of PIL−PIL repulsive interactions causes the extended network to collapse while still maintaining PDMAEMA/PVBBImTf$_2$N block interactions through hydrogen bonding forming overall smaller aggregated structures (Figure 8c) that are still larger than fully extended individual polymer chains. The population aggregates observed in the

14−50 nm range are likely due to rodlike extended polymer chains and charge-shielded collapsed polymer chains where hydrogen bonding was disrupted. Overall, the PDMAEMA-*b*-PVBBImTf$_2$N block copolymer demonstrates self-assembly behavior that can be triggered by the addition of KNO$_3$ salt. Similar salt-triggered self-assembly has been observed for PIL and polyelectrolyte systems, where salt type and concentration influence intermolecular interactions between polyelectrolyte chain segments including charge screening, repulsive interactions, solvophobic chain−chain interactions, and hydrogen bonding.[15,71,83−88]

Film Self-Assembly of PDMAEMA-*b*-PVBBImTf$_2$N Diblock Copolymer. To gather further data on the self-assembly behavior of the PDMAEMA-*b*-PVBBImTf$_2$N block copolymer, a preliminary investigation of the film assembly for the system was also conducted using AFM-IR, a coupled atomic force microscopy-infrared spectroscopic technique. During AFM-IR analysis, a pulsed IR laser illuminates the sample at the AFM cantilever tip, producing a photothermal expansion response that is directly proportional to the IR absorption of the material. This allows for collecting simultaneous chemical images with nanoscale spatial resolution at specific wavenumbers or full spectra at specified points in the AFM image.[89,90] While AFM-IR has previously been used to provide paired nanostructural and chemical composition characterization of different material systems including block copolymers,[91] proteins,[92,93] and nanocomposites,[94,95] to the authors' knowledge, this is the first report of a poly(ionic liquid) system being characterized with AFM-IR.

The film self-assembly of the PDMAEMA-*b*-PVBBImTf$_2$N block copolymer was observed by a solution casting method. In brief, the block copolymer films were prepared by drop-casting ca. 100 μL of the block copolymer solution on piranha-treated silicon wafers followed by thermal annealing at 60 °C for 2 h under vacuum. Due to low solubility and subsequent poor film formation for the block copolymer in pure DMSO solution, only the drop-cast film for PDMAEMA-*b*-PVBBImTf$_2$N in 10 mM KNO$_3$ DMSO solution was characterized. Even so, a film with nonuniform film thickness was formed as shown in Figure S11 in the Supporting Information. Drop-casting films from solutions containing aggregates—as was observed for the block copolymer in 10 mM KNO$_3$ solution by DLS characterization—can result in films with rough surface topography depending on several factors including aggregate size, surface solvophobicity, and
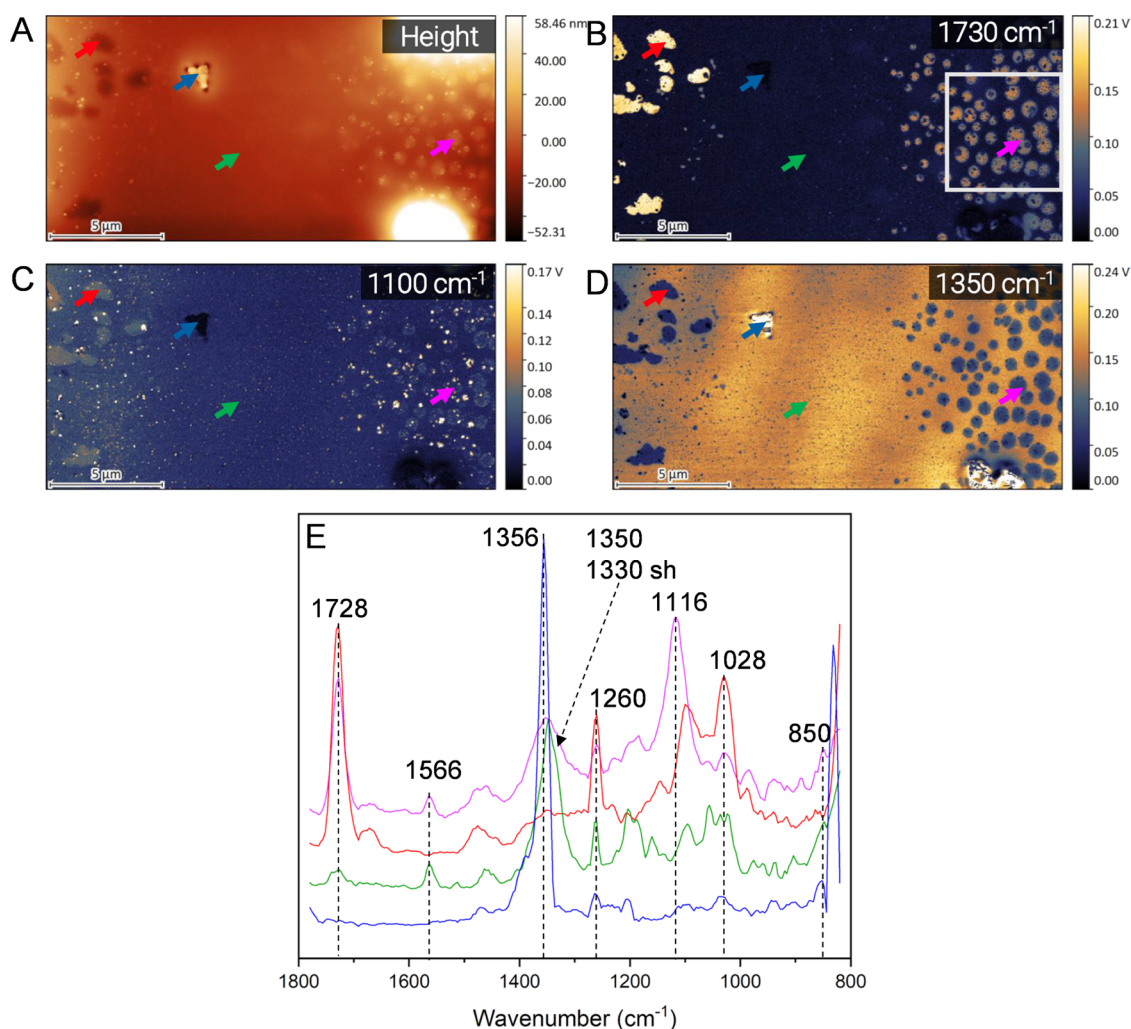
Figure 9. AFM-IR characterization of a 10 μm × 20 μm section of PDMAEMA-*b*-PVBBImTf$_2$N film drop-cast onto a silicon wafer from 10 mM KNO$_3$ DMSO solution including (a) height and chemical IR map traces at (b) 1730 cm^{-1} (C=O str ester PDMAEMA), (c) 1350 cm^{-1} (SO$_2$ asym str of the Tf$_2$N anion), and (d) 1100 cm^{-1} (Si-O silica contaminate). (e) The 10 by 20 μm section of the film located near the edge of the film was analyzed. (e) Point IR spectra were collected at four film locations as indicated by the arrows with the arrow colors (a–d) corresponding to the spectra colors in (e).

capillary effects from solvent drying.[96,97] The solvent solubility issues of the block copolymer and the precipitation of excess KNO$_3$ salts likely lead to the roughness of the film topography. A spin-casting technique to form films with more uniform film thicknesses was also attempted but resulted in irregular and sporadic coverage on the silicon wafer (Figure S12).

Figure 9 shows the AFM height topography and IR chemical maps for a 20 μm × 10 μm section of the drop-cast films located at the edge of the block copolymer film center displaying several different structural features, as indicated by the height trace (Figure 9a). In particular, three different regions were observed: one on the far left with large, depressed deposits or irregular features (marked by a red arrow) at the edge of the film; a homogeneous center section with few topographical features (green arrow); and a section on the right approaching the center of the film with spherical morphology separation (pink arrow). The IR wavenumbers of 1730 cm^{-1} for the PDMAEMA block ester carbonyl stretch (C=O) (Figure 9b) and the Tf$_2$N$^-$ anion SO$_3^-$ asymmetrical stretch (Figure 9c) for the PVBBImTf$_2$N block were selected for chemical mapping to observe microphase separation between the two polymer blocks. The Tf$_2$N$^-$ IR mode was

selected over the imidazolium C=N/C-N bands at 1566 and 1513 cm^{-1} as the Tf$_2$N$^-$ band had greater intensity and greater contrast compared to other IR modes for chemical imaging. Lighter colors in the chemical map traces indicate the presence of the selected IR signal, while dark blue colors indicate either their absence or lower concentration at the analysis penetration depth. Figure 9e displays the point spectra between 1800 and 800 cm^{-1} for each of the spots marked by arrows.

The bright signals produced in Figure 9b (left) (1730 cm^{-1} map) indicate that the ~1 μm by 1 μm irregular depressed deposits contain a large concentration of the C=O str ester band. Taking a point spectrum of one of these features marked by the red arrow and the corresponding red IR spectra trace (Figure 9f) shows an intense peak at 1728 cm^{-1} with no contributions at 1566 cm^{-1} from the imidazolium ring band or at 1350 cm^{-1} from the Tf$_2$N$^-$ anion S=O str band. This suggests that the depressed deposits at the edge of the film are mainly composed of PDMAEMA. As indicated by the NMR 2D DOSY results, the depressed deposits are likely residual PDMAEMA macroinitiator that was not fully removed during the purification of the block copolymer. The large crystalline
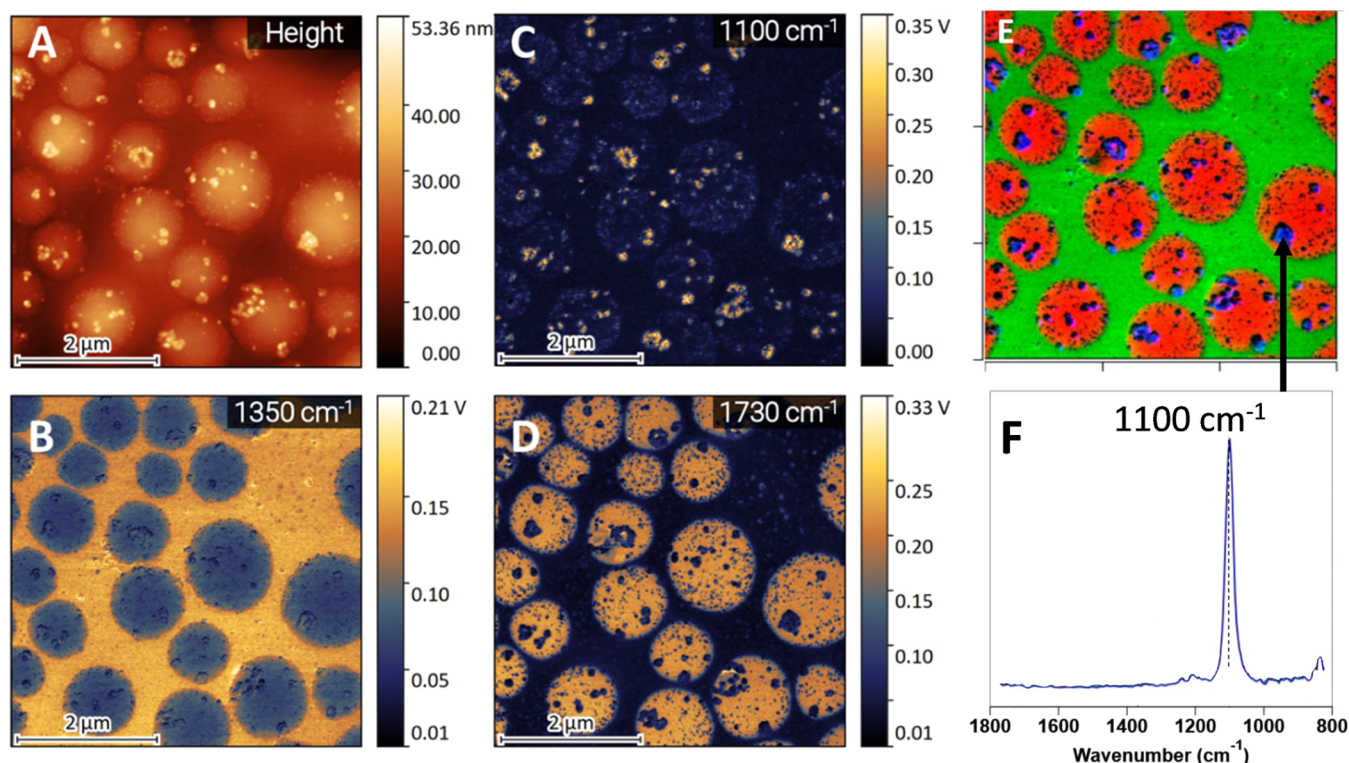
Figure 10. AFM-IR characterization of a 5 μm × 5 μm section of PDMAEMA-*b*-PVBBImTf$_2$N block copolymer drop-cast from 10 mM KNO$_3$ DMSO solution onto silicon wafers. (a) Height trace and several IR traces at (b) 1350 cm^{-1} (SO$_2$ asym str, Tf$_2$N anion), (c) 1100 cm^{-1} (Si-O, silica contaminate), and (d) 1730 cm^{-1} (C=O ester str, PDMAEMA block) indicate microphase separation of the block copolymer. (e) A composite of the IR traces shows PDMAEMA spheres in a PVBBImTf$_2$N matrix with the silica particle contaminants in the hydrophilic PDMAEMA domains. (f) The point spectra trace of one of the silica particle contaminates, indicated by the black arrow in the composite image (e), displays a strong peak at 1100 cm^{-1} typical for Si—O—Si networks.

feature near this section marked by the blue arrow yields an intense peak from excess precipitated KNO$_3$ (1356 cm^{-1}).

The large homogeneous center section is mainly composed of Tf$_2$N$^-$ signals as indicated by the 1350 cm^{-1} chemical map (Figure 9c). Point spectra for the green arrow show contributions from both the PDMAEMA and PVBBImTf$_2$N polymer blocks as indicated by a weaker intensity peak for the PDMAEMA C=O stretch (1730 cm^{-1}) along with stronger peaks for the imidazolium ring (1566 cm^{-1}) and the Tf$_2$N$^-$ anion (1350 cm^{-1}). This indicates that no apparent phase separation of the polymer blocks occurs in this film region. It is noted that tapping AFM-IR probe depth is ca. 50 nm, possibly explaining the presence of both PDMAEMA and PVBBImTf$_2$N IR signals.[98] As the PVBBImTf$_2$N signal is stronger in this center section, there may be stacked lamellae with the more hydrophilic PDMAEMA block interfacing with the hydrophilic piranha-treated SiO$_2$ wafer and the more hydrophobic PVBBImTf$_2$N block at the film surface.

Toward the right side of the height and chemical image maps in Figure 9a–d, a phase-separated spherical morphology is apparent. In the chemical maps, the spherical phases are displayed as yellow in color for the 1730 cm^{-1} map (Figure 9b) and blue in the 1350 cm^{-1} maps (Figure 9c), showing while both polymer blocks are present and contributing to the IR spectra the PDMAEMA block is the major phase as shown by the chemical maps. This is further highlighted by a point spectrum (Figure 9e) of one of the spheres marked by the pink arrow containing peaks for the PDMAEMA carbonyl band (1728 cm^{-1}), imidazolium ring (1566 cm^{-1}), and 1350 cm^{-1} anion. Compared to the homogeneous center section of the

film, the absorbance from the PDMAEMA carbonyl peak (1728 cm^{-1}) is more intense in the spherical phase inclusions, suggesting a higher concentration of the PDMAEMA block. The height scan (Figure 9a) indicates that these spheres are slightly raised from the surrounding morphology, and the phase separation particle diameter size was found to be on average ~ 930 nm (± 240 nm) for the area (within the white box in Figure 9b). These results suggest overall that the spheres are predominately composed of the PDMAEMA block, and these spheres are surrounded by a PVBBImTf$_2$N matrix.

The differences in the morphology observed closer to the film center compared to the phase-separated morphology observed on the left- and right-hand sides of the AFM-IR scans may stem from several factors. For block copolymer films, generally these factors include polymer block compatibility, interactions at the polymer−wafer and polymer−air interfaces, relative molecular weights of the copolymer blocks, and the film thickness in comparison to the periodic structure.[99,100] For the PDMAEMA-*b*-PVBBImTf$_2$N block copolymer, the different morphologies observed are likely due to drop-casting, where relative solvency of the polymer blocks, potential aggregate development in solution and deposition, and the differences in solvent evaporation rate at the edge of the film compared to the center of the film may play roles.[96,97]

Interestingly, the phase separation spheres appeared to contain smaller particle-like features colored dark and bright blue in the 1730 cm^{-1} (Figure 9b) and 1350 cm^{-1} (Figure 9c) maps, respectively. These small particles are showing a high signal intensity (shown as yellow) for the 1100 cm^{-1} (Figure 9d) chemical map. A smaller (5 μm × 5 μm) AFM scan

(marked by the white box in Figure 9b) was taken of this region to allow for a closer examination of these features.

Figure 10 shows the AFM-IR images ($5 \times 5 \ \mu m^2$) collected for the spherical morphology region of the block copolymer film, including the height trace (Figure 10a) and the chemical maps (Figure 10b−d) at 1350 cm^{-1} (SO$_2$ asym str of the Tf$_2$N$^-$ anion), 1100 cm^{-1} (particles), and 1730 cm^{-1} (C=O ester str in PDMAEMA). A composite image of all three traces is compiled in Figure 10e, where the red, green, and blue colors are for the PDMAEMA (1730 cm^{-1}), PVBBImTf$_2$N anion (1350 cm^{-1}), and silica particle (1100 cm^{-1}) signals, respectively. A point spectrum of one of the particles in the PDMAEMA spheres gives a single strong peak at 1100 cm^{-1} (Figure 10f). Based on the spectra, these small particles located within the PDMAEMA spheres are attributed to silica particle contaminants, possibly originating from the Si wafer piranha treatment or due to the solution conditions (nitrate and fluorinated species),[101] which aligns well with the characteristic Si-O-Si stretch at ~1100 cm^{-1}.[102,103] Interestingly, it appears that the silica contaminants selectively interact with the PDMAEMA spheres. This is likely due to the ability of the more hydrophilic PDMAEMA block to form hydrogen bonding interactions between unprotonated tertiary amine groups and the silica −OH groups or through electrostatic binding of protonated amines with the partially negatively charged oxygen groups in silica. Similar behavior has been observed in other amine−silica blends and on silicon surfaces.[104]

The AFM-IR results of the self-assembled film structures indicate that the all-polyelectrolyte PDMAEMA-*b*-PVBBImTf$_2$N block copolymer is capable of both microphase separation and single homogeneous phases at the used process conditions. As processing parameters such as solvent and salt additives, annealing temperature and time, film thickness, and substrate surface properties greatly influence the film morphology of block copolymers,[99,105,106] further exploration of film and membrane processing parameters will be performed in a future work. The AFM-IR findings on the self-assembled film structures showcase the versatile behavior of the all-polyelectrolyte PDMAEMA-*b*-PVBBImTf$_2$N block copolymer, manifesting both microphase separation and homogeneous phases under the investigated processing conditions. Notably, the film morphology of all-polyelectrolyte block copolymers is greatly influenced by processing parameters, including solvent, salt additives, annealing temperature and time, film thickness, and substrate surface properties. Therefore, this all-polyelectrolyte system is ideal for additional investigation into processing parameter impacts to gain deeper insight into the macromolecular design, processing conditions, and control over film and solution assembly.

An interesting finding is that the more hydrophilic PDMAEMA phase can selectively interact with hydrophilic inclusions, such as silica nanoparticles. Potentially this could be leveraged to develop self-assembled composites. For example, these all-polyelectrolyte block copolymers combined with inorganic nanomaterials could allow the weak polyelectrolyte block to selectively coordinate with the nanomaterials while the PIL block is free for application-based functionality, such as ion conductivity or property tunability through ion exchange. Such all-polyelectrolyte block copolymer systems can be useful for producing PILs-based composites for nanoparticle templates or for reinforcing the mechanical properties of solid electrolytes in a variety of electrochemical applications ranging from solid-state battery electrolytes to ionic actuators and sensors.

■ CONCLUSIONS

A novel all-polyelectrolyte block copolymer composed of a poly(ionic liquid) block and a tertiary amine-based weak polyelectrolyte was successfully synthesized through Cu(0)-mediated atom transfer radical polymerization. Living control of a well-defined PDMAEMA macroinitiator was confirmed with a degree of polymerization of 45 units and PDI of ~1.41. While living control of the PIL block was not confirmed, FTIR, ^{1}HNMR, and NMR DOSY spectroscopies provide compelling evidence of the successful synthesis and connectivity of the PDMAEMA-*b*-PVBBImTf$_2$N block copolymer with an estimated ~67 PIL unit degree of polymerization. Differences in the supramolecular environment between the PIL homopolymer and block copolymer were examined with FTIR and ^{1}H NMR spectroscopies in the bulk and in solution, respectively. While no differences were observed in the bulk, the block copolymer exhibited both hydrogen bonding and electrostatic interactions in DMSO and KNO$_3$-DMSO solutions, as demonstrated by shifts in the imidazolium C$_2$-H proton and the PDMAEMA block methyl and methylene groups. DLS measurements of the block copolymer indicate that an extended network-like structure is formed in pure DMSO as a result of combined hydrogen bonding between the PDMAEMA and PVBBIMTf$_2$N blocks and repulsive interactions between positively charged groups on the polymer chain. The addition of 10 mM KNO$_3$ sufficiently screens these repulsive interactions, leading to a collapse in the polymer network-like structure while preserving hydrogen bonding interactions as suggested by the NMR shifts of the imidazolium C$_2$-H and PDMAEMA methyl groups in 10 mM KNO$_3$ DMSO solution. The film assembly of the all-polyelectrolyte block copolymer film was interrogated for the first time by AFM-IR, which revealed diverse surface morphologies, including a distinct spherical phase separation of PDMAEMA from the PVBBImTf$_2$N. Intriguingly, silica nanoparticles were found to selectively interact with the PDMAEMA spheres, indicating a wide range of potential applications of the PDMAEMA-*b*-PVBBImTf$_2$N block copolymer including inorganic nanoparticle−polymer composites as well as the design of diverse materials for drug delivery systems, nanoelectronics, and energy storage systems.

■ MATERIALS AND METHODS

Materials. 1-Butylimidazole, 4-chloromethylsytrene, and lithium bis(trifluoromethylsulfonyl)imide (**LiTf$_2$N**) were purchased from TCI America. Acetonitrile, dimethylsulfoxide (**DMSO**), and ethyl acetate were purchased from VWR. Diethyl ether was purchased from Beantown Chemical. N,N-Dimethylformamide (**DMF**) was purchased from Alfa Aesar. N,N,N′,N″,N″-Pentamethyl-diethylenetriamine (**PMDETA**), methyl 2-bromopropionate (**MBP**), copper (II) bromide (**CuBr$_2$**), 2-(dimethylamino) ethyl methacrylate (**DMAEMA**), tris (2-pyridylmethyl) amine (**TPMA**), hydrochloric acid, α-bromophenylacetic acid (**α-BPA**), and potassium nitrate (**KNO$_3$**) were purchased from Aldrich. DMSO-d_6 was purchased from the University of Oklahoma Chemistry Stockroom. All purchased chemicals were used as received.

General 4-Vinylbenzyl-3-butylimidazolium Chloride Synthesis (VBBImCl). 1-Butylimidazole (~11 mL) and 4-

chloromethylstyrene (~10 mL) were dissolved in 40 mL of acetonitrile. The mixture was allowed to react at 40 °C for 24 h under stirring. The reaction was then allowed to cool to room temperature and then stirred for an additional 24 h at 20 °C. The product solution was concentrated with a rotary evaporator at 40 °C. The concentrated solution was poured into 100 mL of diethyl ether. A yellow transparent oil was collected immediately at the bottom of the flask. The diethyl ether was decanted, and additional fresh diethyl ether (40 mL × 3 times) was added to wash the product. Finally, the IL was dried in the vacuum oven at room temperature overnight.

General 4-Vinylbenzyl-3-butylimidazolium Bis-(trifluoromethylsulfonyl)imide (VBBImTf$_2$N) Synthesis. The VBBImCl product was dissolved in 150 mL of Millipore water under vigorous stirring. 20.1 g of LiTf$_2$N was added to the reaction mixture under stirring. The product immediately precipitated and accumulated at the bottom of the flask. The solution was transferred to a 500 mL round-bottom flask, and the precipitated IL was dissolved in 250 mL of ethyl acetate under vigorous stirring. This ethyl acetate solution was added to the 500 mL round-bottom flask and was then vigorously stirred to form a yellow-white emulsion. The biphasic reaction mixture was stirred at room temperature for 24 h. Afterward, the stirring was stopped and the mixture was allowed to separate into two phases. Product from the aqueous layer was extracted with 50 mL of ethyl acetate (3x), and the organic phase was combined with the original ethyl acetate product phase. The total ethyl acetate product layer was then washed with 50 mL of Millipore water (3x). Ethyl acetate was removed by a rotary evaporator and dried in the vacuum oven at ~35 °C to remove trace ethyl acetate.

General Cu(0)-Mediated ATRP Synthesis of Poly[4-vinylbenzyl-3-butylimidazolium bis-(trifluoromethylsulfonyl)imide] (PVBBImTf$_2$N). VBBImTf$_2$N monomer (2.32 g) was dissolved in (7 mL) DMF in a test tube for 30 min. CuBr$_2$ deactivator (0.002 g) was added to a separate dry test tube. The dissolved monomer, PMDETA ligand (12.4 μL), and MBP initiator (1.88 μL) were added to the test tube in that order. After adding the MBP, the test tube was quickly capped with a septum and frozen in liquid nitrogen. At least 4 freeze−pump−thaw cycles were performed to degas the solution. A 4 cm long Cu(0) wire was treated in a 6 M HCl/methanol solution under nitrogen before removing the acid solution with a syringe and drying with nitrogen. The treated Cu(0) wire was added to the reaction test tube during the last freeze cycle. Three cycles of vacuum and backfilling with nitrogen gas were performed while the solution was frozen. The test tube was then allowed to thaw to room temperature and was then transferred to an oil bath at 90 °C under nitrogen for 24 h. 100 μL samples were taken periodically to track monomer conversion. The polymerization was stopped by exposing the system to air. A 10 mL solution of a 4:1 volume ratio of methanol to water was used to precipitate the polymer product.

Cu(0)-Mediated ATRP Synthesis of Poly[2-(dimethylamino)ethyl methacrylate] (PDMAEMA) Macroinitiator. The Cu(0)-mediated ATRP synthesis of the PDMAEMA macroinitiator was performed similarly to a previous work by the authors' group and is briefly described here.[34] DMAEMA (2.5 mL), CuBr$_2$ (0.0168 g), TPMA (0.035 g), NaCl (0.248 g), α-BPA (~0.064 g), and 3 mL of water were added to a test tube. The pH of the solution was adjusted to ~8.6 by adding 2.5 mL of 1 M HCl solution. At least 4 freeze−pump−thaw cycles were performed, and the 6.5 cm long Cu(0) wire and magnetic stirrer were added on the last freeze cycle. A 4 cm long Cu(0) wire had been pretreated in 1 M HCl/methanol solution as described previously. Three cycles of backfilling with nitrogen and vacuuming were done. The solution was allowed to thaw and then was added to a water bath maintained at 2 °C. The reaction was allowed to proceed for ~5 h, and then the reaction was stopped by exposing the solution to air and adding ammonium sulfate directly to the reaction mixture to precipitate the product. The polymer was dissolved in methanol and separated from the ammonium sulfate through vacuum filtration before washing with methanol. The methanol was then evaporated, and the polymer was dried in the vacuum oven to remove trace solvent.

Cu(0)-Mediated ATRP Synthesis of Poly(2-(dimethylamino)ethyl methacrylate-*block*-[Poly(4-vinylbenzyl-3-butylimidazolium bis(trifluoromethane)-sulfonylimide] Block Copolymer (PDMAEMA-*b*-PVBBImTf$_2$N). VBBImTf$_2$N monomer (1.61 g) and PDMAEMA macroinitiator (0.24 g) were weighed out and dissolved separately in 4 mL and 2 mL of DMF, respectively. To a dry test tube, the CuBr$_2$ (0.0021 g) deactivator, PMDETA ligand (25 μL), and a magnetic stirrer were added. The monomer and macroinitiator solutions were then added to this test tube. Four FPT cycles were performed followed by the addition of a 4 cm long Cu(0) copper wire after the last cycle. The system was backfilled and vacuumed (3x) before thawing the solution under nitrogen and adding it to the 90 °C oil bath and allowed to react for 24 h. Small 100 μL aliquots were collected periodically to track polymerization conversion and chain growth. The reaction was stopped by exposure to air. The product was precipitated in excess chloroform and washed (3x) with additional chloroform. The final product, PDMAEMA-*b*-PVBBImTf$_2$N, was dried in a vacuum oven to remove residual solvent.

Characterizations. ATR FTIR was carried out on a Nicolet iS50R FT IR spectrometer with a DLaTGS detector at a resolution of 4 cm^{-1} for 64 or 256 scans. ^{1}HNMR and Oneshot DOSY (DONESHOT) experiments were performed for the produced polymers on a Varian VNMRS 500 MHz NMR spectrometer at the (University of Oklahoma NMR Facility). Spectra were referenced at the DMSO-d_5 peak at 2.5 ppm. Polymerization conversion was determined by ratioing the monomer vinyl group peak integral to a select polymer peak integral. The degree of polymerization (DP) for the PDMAEMA macroinitiator was determined by ratioing the integral of one of the methylene peaks (~4.08 ppm) in the monomer unit to the benzyl chain end group (ca. 7.18−7.18 ppm) integral. The degree of polymerization for the block copolymer was determined by ratioing the PVBBImTf$_2$N benzyl peak integral (5.98−6.71 ppm) to the macroinitiator PDMAEMA tertiary amine methyl group peak integral (2.52−2.35 ppm). Unfortunately, due to overlapping signals of the PVBBImTf$_2$N chain signals with the end group signals, the DP could not be determined for the PVBBImTf$_2$N homopolymer. One-dimensional spectra collected in the DONESHOT experiment were converted to a 2D DOSY through a Bayesian transformation method using the MNova software package. A Shimadzu Prominence HPLC equipped with a Waters R410 differential refractometer and a Wyatt DAWN F light scattering detector was used to characterize the PDMAEMA macroinitiator molecular weight and polydispersity index (PDI) relative to poly(ethylene glycol) standards. The

instrument used Aquagel-OH Mixed H and Aquagel-OH 30 columns, and the mobile phase was a 0.3 M sodium acetate solution at a pH of 4 containing 0.15 M triethylamine to suppress polymer−column interactions. Dynamic light scattering (DLS) was performed with a NanoBrook Omni using a 90° detector. Either double-exponential (Dblexp) or non-negatively constrained least squares (NNLS) fitting models were used as appropriate for each sample. Example fittings using each model are provided in the Supporting Information (Figures S4 and S5). Eight measurements were performed per sample. Atomic force microscopy with an FTIR module (AFM-IR) of the PDMAEMA-*b*-PVBBImTf$_2$N block copolymer film was performed using a Bruker NanoIR3 System equipped with a Mircat-QT laser (Daylight Solutions). The system was operated in tapping AFM-IR mode using a PR-EX-TNIR-A-10 probe (4 N/m, 60 kHz nominal resonance frequency), the pulse rate of the IR laser was chosen to be the difference frequency of the first 2 cantilever resonance frequencies (∼300 kHz). PDMAEMA-*b*-PVBBImTf$_2$N block copolymer in 10 mM KNO$_3$ DMSO solution was drop-cast on to a silicon wafer that had been pretreated with piranha solution and UV-ozone cleaning. The films were dried in the vacuum oven at 60 °C for ∼2 h prior to AFM-IR analysis. A Nikon Eclipse LV100D optical microscope equipped with a Lumenera Scientific Infinity digital camera was used to obtain optical microscopy images of the block copolymer in DMSO solution.

ASSOCIATED CONTENT

Supporting Information

The Supporting Information is available free of charge at https://pubs.acs.org/doi/10.1021/acsomega.3c03989.

1D DONESHOT DOSY array of the PDMAEMA-*b*-PVBBImTf$_2$N block copolymer and ^{1}H NMR spectra of the PDMAEMA macroinitiator using NMR characterization; additional solubility data of the PVBBImTf$_2$N homopolymer and PDMAEMA-*b*-PVBBImTf$_2$N block copolymer; dynamic light scattering (DLS) correlation functions and intensity-based hydrodynamic diameters in pure DMSO and 10 mM KNO$_3$ DMSO solution and different model fitting of the correlation functions for the PVBBImTf$_2$N homopolymer and PDMAEMA-*b*-PVBBImTf$_2$N block copolymer in pure DMSO and 10 mM KNO$_3$; DLS salt study with the DLS correlation funtion and hydrodynamic diameters of the block copolymer solvation in DMSO and KNO$_3$ DMSO solutions; photographs and optical microscopy images of the block copolymer in pure DMSO and for different KNO$_3$ salt concentrations; photograph of gel-like behavior in pure DMSO solvent; and photographs and optical microscopy images of the block copolymer films drop-casted and spin-coated on silicon wafers from 10 mM KNO$_3$ DMSO solution (PDF)

Video of the block copolymer in 15 mM KNO$_3$ DMSO showing collapsed structure (MP4)

AUTHOR INFORMATION

Corresponding Author

Keisha B. Walters − *Ralph E. Martin Department of Chemical Engineering, University of Arkansas, Fayetteville, Arkansas 72701, United States;* orcid.org/0000-0002-0875-2659; Phone: 479-575-4951; Email: keishaw@uark.edu

Author

Kayla Foley − *Ralph E. Martin Department of Chemical Engineering, University of Arkansas, Fayetteville, Arkansas 72701, United States;* orcid.org/0000-0003-4316-6011

Complete contact information is available at:
https://pubs.acs.org/10.1021/acsomega.3c03989

Notes

The authors declare no competing financial interest.

ACKNOWLEDGMENTS

REFERENCES

(1) Qian, W.; Texter, J.; Yan, F. Frontiers in poly(ionic liquid)s: synthesis and applications. *Chem. Soc. Rev.* **2017**, *46*, 1124−1159.

(2) O'Harra, K. E.; Timmermann, G. M.; Bara, J. E.; Miller, K. M. Designing Ionic Liquid-Derived Polymer Composites from Poly(Ionic Liquid)−Ionene Semi-interpenetrating Networks. *ACS Appl. Polym. Mater.* **2021**, *3*, 1995−2004.

(3) Yuan, J.; Mecerreyes, D.; Antonietti, M. Poly(ionic liquid)s: An update. *Prog. Polym. Sci.* **2013**, *38*, 1009−1036.

(4) Ajjan, F. N.; Ambrogi, M.; Tiruye, G. A.; Cordella, D.; Fernandes, A. M.; Grygiel, K.; Isik, M.; Patil, N.; Porcarelli, L.; Rocasalbas, G.; et al. Innovative polyelectrolytes/poly(ionic liquid)s for energy and the environment. *Polym. Int.* **2017**, *66*, 1119−1128.

(5) Yuan, J.; Antonietti, M. Poly(Ionic Liquid)s as Ionic Liquid-Based Innovative Polyelectrolytes. In *Applications of Ionic Liquids in Polymer Science and Technology*; Mecerreyes, D., Ed.; Springer Berlin Heidelberg, 2015; pp 47−67.

(6) Barrulas, R. V.; Zanatta, M.; Casimiro, T.; Corvo, M. C. Advanced porous materials from poly(ionic liquid)s: Challenges, applications and opportunities. *Chem. Eng. J.* **2021**, *411*, No. 128528.

(7) Sun, J.-K.; Kochovski, Z.; Zhang, W.-Y.; Kirmse, H.; Lu, Y.; Antonietti, M.; Yuan, J. General Synthetic Route toward Highly Dispersed Metal Clusters Enabled by Poly(ionic liquid)s. *J. Am. Chem. Soc.* **2017**, *139*, 8971−8976.

(8) Zhang, S.-Y.; Zhuang, Q.; Zhang, M.; Wang, H.; Gao, Z.; Sun, J.-K.; Yuan, J. Poly(ionic liquid) composites. *Chem. Soc. Rev.* **2020**, *49*, 1726−1755.

(9) Choi, J.-H.; Ye, Y.; Elabd, Y. A.; Winey, K. I. Network Structure and Strong Microphase Separation for High Ion Conductivity in Polymerized Ionic Liquid Block Copolymers. *Macromolecules* **2013**, *46*, 5290−5300.

(10) Eshetu, G. G.; Mecerreyes, D.; Forsyth, M.; Zhang, H.; Armand, M. Polymeric ionic liquids for lithium-based rechargeable batteries. *Mol. Syst. Des. Eng.* **2019**, *4*, 294−309.

(11) Margaretta, E.; Fahs, G. B.; Inglefield, D. L., Jr.; Jangu, C.; Wang, D.; Heflin, J. R.; Moore, R. B.; Long, T. E. Imidazolium-Containing ABA Triblock Copolymers as Electroactive Devices. *ACS Appl. Mater. Interfaces* **2016**, *8*, 1280−1288.

(12) Shi, Z.; Newell, B. S.; Bailey, T. S.; Gin, D. L. Ordered, microphase-separated, noncharged-charged diblock copolymers via the sequential ATRP of styrene and styrenic imidazolium monomers. *Polymer* **2014**, *55*, 6664−6671.

(13) Wu, B.; Zhang, W.; Gao, N.; Zhou, M.; Liang, Y.; Wang, Y.; Li, F.; Li, G. Poly (ionic liquid)-Based Breath Figure Films: A New Kind

of Honeycomb Porous Films with Great Extendable Capability. *Sci. Rep.* **2017**, *7*, No. 13973.

(14) He, H.; Zhong, M.; Adzima, B.; Luebke, D.; Nulwala, H.; Matyjaszewski, K. A Simple and Universal Gel Permeation Chromatography Technique for Precise Molecular Weight Characterization of Well-Defined Poly(ionic liquid)s. *J. Am. Chem. Soc.* **2013**, *135*, 4227–4230.

(15) Luo, H.; Tang, Q.; Zhong, J.; Lei, Z.; Zhou, J.; Tong, Z. Interplay of Solvation and Size Effects Induced by the Counterions in Ionic Block Copolymers on the Basis of Hofmeister Series. *Macromol. Chem. Phys.* **2019**, *220*, No. 1800508.

(16) Vijayakrishna, K.; Jewrajka, S. K.; Ruiz, A.; Marcilla, R.; Pomposo, J. A.; Mecerreyes, D.; Taton, D.; Gnanou, Y. Synthesis by RAFT and Ionic Responsiveness of Double Hydrophilic Block Copolymers Based on Ionic Liquid Monomer Units. *Macromolecules* **2008**, *41*, 6299–6308.

(17) Yang, Y.; Li, X.; Yan, Y.; Pan, R.; Liu, J.; Lian, M.; Luo, X.; Liu, G. RAFT polymerization-induced self-assembly of poly(ionic liquid. *e-Polymers* **2022**, *22*, 803–808.

(18) Yang, Y.; Zheng, J.; Man, S.; Sun, X.; An, Z. Synthesis of poly(ionic liquid)-based nano-objects with morphological transitions via RAFT polymerization-induced self-assembly in ethanol. *Polym. Chem.* **2018**, *9*, 824–827.

(19) He, H.; Rahimi, K.; Zhong, M.; Mourran, A.; Luebke, D. R.; Nulwala, H. B.; Möller, M.; Matyjaszewski, K. Cubosomes from hierarchical self-assembly of poly(ionic liquid) block copolymers. *Nat. Commun.* **2017**, *8*, No. 14057.

(20) Mai, Y.; Eisenberg, A. Self-assembly of block copolymers. *Chem. Soc. Rev.* **2012**, *41*, 5969–5985.

(21) Green, M. D.; Wang, D.; Hemp, S. T.; Choi, J.-H.; Winey, K. I.; Heflin, J. R.; Long, T. E. Synthesis of imidazolium ABA triblock copolymers for electromechanical transducers. *Polymer* **2012**, *53*, 3677–3686.

(22) Jangu, C.; Wang, J.-H. H.; Wang, D.; Sharick, S.; Heflin, J. R.; Winey, K. I.; Colby, R. H.; Long, T. E. Well-Defined Imidazolium ABA Triblock Copolymers as Ionic-Liquid-Containing Electroactive Membranes. *Macromol. Chem. Phys.* **2014**, *215*, 1319–1331.

(23) Cordella, D.; Kermagoret, A.; Debuigne, A.; Jerome, C.; Mecerreyes, D.; Isik, M.; Taton, D.; Detrembleur, C. All Poly(ionic liquid)-Based Block Copolymers by Sequential Controlled Radical Copolymerization of Vinylimidazolium Monomers. *Macromolecules* **2015**, *48*, 5230–5243.

(24) Cordella, D.; Debuigne, A.; Jérôme, C.; Kochovski, Z.; Taton, D.; Detrembleur, C. One-Pot Synthesis of Double Poly(Ionic Liquid) Block Copolymers by Cobalt-Mediated Radical Polymerization-Induced Self-Assembly (CMR-PISA) in Water. *Macromol. Rapid Commun.* **2016**, *37*, 1181–1187. (acccessed 2023/04/11).

(25) Cordella, D.; Ouhib, F.; Aqil, A.; Defize, T.; Jérôme, C.; Serghei, A.; Drockenmuller, E.; Aissou, K.; Taton, D.; Detrembleur, C. Fluorinated Poly(ionic liquid) Diblock Copolymers Obtained by Cobalt-Mediated Radical Polymerization-Induced Self-Assembly. *ACS Macro Lett.* **2017**, *6*, 121–126.

(26) Depoorter, J.; Yan, X.; Zhang, B.; Sudre, G.; Charlot, A.; Fleury, E.; Bernard, J. All poly(ionic liquid) block copolymer nanoparticles from antagonistic isomeric macromolecular blocks via aqueous RAFT polymerization-induced self-assembly. *Polym. Chem.* **2021**, *12*, 82–91.

(27) Kawauchi, Y.; Kouka, A.; Guragain, S.; Bastakoti, B. P.; Yusa, S.-i.; Nakashima, K. Schizophrenic micelles of poly(3-(methacryloylamino)propyltrimethylammonium chloride-b-2-(dimethylamino)ethyl methacrylate) in aqueous solutions. *Colloids Surf., A* **2013**, *434*, 56–62.

(28) Zhang, B.; Yan, X.; Alcouffe, P.; Charlot, A.; Fleury, E.; Bernard, J. Aqueous RAFT Polymerization of Imidazolium-Type Ionic Liquid Monomers: En Route to Poly(ionic liquid)-Based Nanoparticles through RAFT Polymerization-Induced Self-Assembly. *ACS Macro Lett.* **2015**, *4*, 1008–1011.

(29) Sanchez-Ballester, N. M.; Sciortino, F.; Mir, S. H.; Rydzek, G. Weak Polyelectrolytes as Nanoarchitectonic Design Tools for

Functional Materials: A Review of Recent Achievements. *Molecules* **2022**, *27*, 3263.

(30) Lu, Y.; Zhuk, A.; Xu, L.; Liang, X.; Kharlampieva, E.; Sukhishvili, S. A. Tunable pH and temperature response of weak polyelectrolyte brushes: role of hydrogen bonding and monomer hydrophobicity. *Soft Matter* **2013**, *9*, 5464–5472.

(31) Vijayakrishna, K.; Mecerreyes, D.; Gnanou, Y.; Taton, D. Polymeric Vesicles and Micelles Obtained by Self-Assembly of Ionic Liquid-Based Block Copolymers Triggered by Anion or Solvent Exchange. *Macromolecules* **2009**, *42*, 5167–5174.

(32) Banerjee, P.; Anas, M.; Jana, S.; Mandal, T. K. Recent developments in stimuli-responsive poly(ionic liquid)s. *J. Polym. Res.* **2020**, *27*, 177.

(33) Anastasaki, A.; Nikolaou, V.; Nurumbetov, G.; Wilson, P.; Kempe, K.; Quinn, J. F.; Davis, T. P.; Whittaker, M. R.; Haddleton, D. M. Cu(0)-Mediated Living Radical Polymerization: A Versatile Tool for Materials Synthesis. *Chem. Rev.* **2016**, *116*, 835–877.

(34) Britten, C. N.; Lason, K.; Walters, K. B. Facile Synthesis of Tertiary Amine Pendant Polymers by Cu0-Mediated ATRP under Aqueous Conditions. *Macromolecules* **2021**, *54*, 10360–10369.

(35) Konkolewicz, D.; Wang, Y.; Krys, P.; Zhong, M.; Isse, A. A.; Gennaro, A.; Matyjaszewski, K. SARA ATRP or SET-LRP. End of controversy? *Polym. Chem.* **2014**, *5*, 4396–4417.

(36) Mendonça, P. V.; Konkolewicz, D.; Averick, S. E.; Serra, A. C.; Popov, A. V.; Guliashvili, T.; Matyjaszewski, K.; Coelho, J. F. J. Synthesis of cationic poly((3-acrylamidopropyl)trimethylammonium chloride) by SARA ATRP in ecofriendly solvent mixtures. *Polym. Chem.* **2014**, *5*, 5829–5836.

(37) Mohammadi, M.; Salami-Kalajahi, M.; Roghani-Mamaqani, H.; Golshan, M. Effect of molecular weight and polymer concentration on the triple temperature/pH/ionic strength-sensitive behavior of poly(2-(dimethylamino)ethyl methacrylate). *Int. J. Polym. Mater. Polym. Biomater.* **2017**, *66*, 455–461.

(38) Laaser, J. E.; Jiang, Y.; Sprouse, D.; Reineke, T. M.; Lodge, T. P. pH- and Ionic-Strength-Induced Contraction of Polybasic Micelles in Buffered Aqueous Solutions. *Macromolecules* **2015**, *48*, 2677–2685.

(39) Hunley, M. T.; England, J. P.; Long, T. E. Influence of Counteranion on the Thermal and Solution Behavior of Poly(2-(dimethylamino)ethyl methacrylate)-Based Polyelectrolytes. *Macromolecules* **2010**, *43*, 9998–10005.

(40) Karjalainen, E.; Aseyev, V.; Tenhu, H. Influence of Hydrophobic Anion on Solution Properties of PDMAEMA. *Macromolecules* **2014**, *47*, 2103–2111.

(41) Agudelo, N. A.; Elsen, A. M.; He, H.; López, B. L.; Matyjaszewski, K. ABA triblock copolymers from two mechanistic techniques: Polycondensation and atom transfer radical polymerization. *J. Polym. Sci., Part A: Polym. Chem.* **2015**, *53*, 228–238.

(42) Chi, W. S.; Hong, S. U.; Jung, B.; Kang, S. W.; Kang, Y. S.; Kim, J. H. Synthesis, structure and gas permeation of polymerized ionic liquid graft copolymer membranes. *J. Membr. Sci.* **2013**, *443*, 54–61.

(43) He, H.; Luebke, D.; Nulwala, H.; Matyjaszewski, K. Synthesis of Poly(ionic liquid)s by Atom Transfer Radical Polymerization with ppm of Cu Catalyst. *Macromolecules* **2014**, *47*, 6601–6609.

(44) Ydens, I.; Moins, S.; Degée, P.; Dubois, P. Solution properties of well-defined 2-(dimethylamino)ethyl methacrylate-based (co)-polymers: A viscometric approach. *Eur. Polym. J.* **2005**, *41*, 1502–1509.

(45) Shim, Y.-H.; Bougard, F.; Coulembier, O.; Lazzaroni, R.; Dubois, P. Synthesis and characterization of original 2-(dimethylamino)ethyl methacrylate/poly(ethyleneglycol) star-copolymers. *Eur. Polym. J.* **2008**, *44*, 3715–3723.

(46) Izunobi, J. U.; Higginbotham, C. L. Polymer Molecular Weight Analysis by 1H NMR Spectroscopy. *J. Chem. Educ.* **2011**, *88*, 1098–1104.

(47) Abdelghafour, M. M.; Orbán, Á.; Deák, Á.; Lamch, Ł.; Frank, É.; Nagy, R.; Ádám, A.; Sipos, P.; Farkas, E.; Bari, F.; et al. The Effect of Molecular Weight on the Solubility Properties of Biocompatible Poly(ethylene succinate) Polyester. *Polymers* **2021**, *13*, 2725.

(48) Karjalainen, E.; Chenna, N.; Laurinmäki, P.; Butcher, S. J.; Tenhu, H. Diblock copolymers consisting of a polymerized ionic liquid and poly(N-isopropylacrylamide). Effects of PNIPAM block length and counter ion on self-assembling and thermal properties. *Polym. Chem.* **2013**, *4*, 1014−1024.

(49) May, A. W.; Shi, Z.; Wijayasekara, D. B.; Gin, D. L.; Bailey, T. S. Self-assembly of highly asymmetric, poly(ionic liquid)-rich diblock copolymers and the effects of simple structural modification on phase behaviour. *Polym. Chem.* **2019**, *10*, 751−765.

(50) Yuan, J.; Schlaad, H.; Giordano, C.; Antonietti, M. Double hydrophilic diblock copolymers containing a poly(ionic liquid) segment: Controlled synthesis, solution property, and application as carbon precursor. *Eur. Polym. J.* **2011**, *47*, 772−781.

(51) He, H.; Zhong, M.; Luebke, D.; Nulwala, H.; Matyjaszewski, K. Atom transfer radical polymerization of ionic liquid monomer: The influence of salt/counterion on polymerization. *J. Polym. Sci., Part A: Polym. Chem.* **2014**, *52*, 2175−2184.

(52) Matyjaszewski, K.; Xia, J. Atom Transfer Radical Polymerization. *Chem. Rev.* **2001**, *101*, 2921−2990.

(53) Roth, C.; Chatzipapadopoulos, S.; Kerlé, D.; Friedriszik, F.; Lütgens, M.; Lochbrunner, S.; Kühn, O.; Ludwig, R. Hydrogen bonding in ionic liquids probed by linear and nonlinear vibrational spectroscopy. *New J. Phys.* **2012**, *14*, No. 105026.

(54) Paschoal, V. H.; Faria, L. F. O.; Ribeiro, M. C. C. Vibrational Spectroscopy of Ionic Liquids. *Chem. Rev.* **2017**, *117*, 7053−7112.

(55) Grondin, J.; Lassègues, J.-C.; Cavagnat, D.; Buffeteau, T.; Johansson, P.; Holomb, R. Revisited vibrational assignments of imidazolium-based ionic liquids. *J. Raman Spectrosc.* **2011**, *42*, 733−743.

(56) Hunt, P. A.; Ashworth, C. R.; Matthews, R. P. Hydrogen bonding in ionic liquids. *Chem. Soc. Rev.* **2015**, *44*, 1257−1288.

(57) Katsyuba, S. A.; Dyson, P. J.; Vandyukova, E. E.; Chernova, A. V.; Vidiš, A. Molecular Structure, Vibrational Spectra, and Hydrogen Bonding of the Ionic Liquid 1-Ethyl-3-methyl-1H-imidazolium Tetrafluoroborate. *Helv. Chim. Acta* **2004**, *87*, 2556−2565.

(58) Larkin, P. J. IR and Raman Spectra−Structure Correlations: Characteristic Group Frequencies. In *Infrared and Raman Spectroscopy*, 2nd ed.; Larkin, P. J., Ed.; Elsevier, 2018; pp 85−134.

(59) Coates, J. Interpretation of Infrared Spectra, A Practical Approach. In *Encyclopedia of Analytical Chemistry*, 2006.

(60) Socrates, G. *Infrared and Raman Characteristic Group Frequencies Tables and Charts*; John Wiley & Sons, LTD, 2001.

(61) Silverstein, R. M.; W, F. X.; Kiemle, D. J.; Bryce, D. L. *Spectrometric Identification of Organic Compounds*, Wiley: 2014.

(62) Mikol, V.; Rodeau, J.-L.; Giegé, R. Changes of pH during biomacromolecule crystallization by vapor diffusion using ammonium sulfate as the precipitant. *J. Appl. Crystallogr.* **1989**, *22*, 155−161.

(63) Ni, P.; Zhang, M.; Ma, L.; Fu, S. Poly(dimethylamino)ethyl Methacrylate for Use as a Surfactant in the Miniemulsion Polymerization of Styrene. *Langmuir* **2006**, *22*, 6016−6023.

(64) Kiefer, J.; Fries, J.; Leipertz, A. Experimental vibrational study of imidazolium-based ionic liquids: Raman and infrared spectra of 1-ethyl-3-methylimidazolium bis(trifluoromethylsulfonyl)imide and 1-ethyl-3-methylimidazolium ethylsulfate. *Appl. Spectrosc.* **2007**, *61*, 1306−1311.

(65) James, C.; Ravikumar, C.; Jayakumar, V. S.; Hubert Joe, I. Vibrational spectra and potential energy distributions for 1-benzyl-1H-imidazole by normal coordinate analysis. *J. Raman Spectrosc.* **2009**, *40*, 537−545.

(66) Noack, K.; Schulz, P. S.; Paape, N.; Kiefer, J.; Wasserscheid, P.; Leipertz, A. The role of the C2 position in interionic interactions of imidazolium based ionic liquids: a vibrational and NMR spectroscopic study. *Phys. Chem. Chem. Phys.* **2010**, *12*, 14153−14161.

(67) Long, B. Experimental Studies and Thermodynamic Modeling of the Solubilities of Potassium Nitrate, Potassium Chloride, Potassium Bromide, and Sodium Chloride in Dimethyl Sulfoxide. *Ind. Eng. Chem. Res.* **2011**, *50*, 7019−7026.

(68) Cui, J.; Nie, F.-M.; Yang, J.-X.; Pan, L.; Ma, Z.; Li, Y.-S. Novel imidazolium-based poly(ionic liquid)s with different counterions for self-healing. *J. Mater. Chem. A* **2017**, *5*, 25220−25229.

(69) Cremer, T.; Kolbeck, C.; Lovelock, K. R. J.; Paape, N.; Woelfel, R.; Schulz, P. S.; Wasserscheid, P.; Weber, H.; Thar, J.; Kirchner, B.; et al. Towards a Molecular Understanding of Cation-Anion Interactions-Probing the Electronic Structure of Imidazolium Ionic Liquids by NMR Spectroscopy, X-ray Photoelectron Spectroscopy and Theoretical Calculations. *Chem. - Eur. J.* **2010**, *16*, 9018−9033.

(70) Matthews, R. P.; Villar-Garcia, I. J.; Weber, C. C.; Griffith, J.; Cameron, F.; Hallett, J. P.; Hunt, P. A.; Welton, T. A structural investigation of ionic liquid mixtures. *Phys. Chem. Chem. Phys.* **2016**, *18*, 8608−8624.

(71) Guo, J.; Zhou, Y.; Qiu, L.; Yuan, C.; Yan, F. Self-assembly of amphiphilic random co-poly(ionic liquid)s: the effect of anions, molecular weight, and molecular weight distribution. *Polym. Chem.* **2013**, *4*, 4004−4009.

(72) Chen, S.-C.; Kuo, S.-W.; Liao, C.-S.; Chang, F.-C. Syntheses, Specific Interactions, and pH-Sensitive Micellization Behavior of Poly[vinylphenol-b-2-(dimethylamino)ethyl methacrylate] Diblock Copolymers. *Macromolecules* **2008**, *41*, 8865−8876.

(73) Yuk, S. H.; Cho, S. H.; Lee, S. H. pH/Temperature-Responsive Polymer Composed of Poly((N,N-dimethylamino)ethyl methacrylate-co-ethylacrylamide). *Macromolecules* **1997**, *30*, 6856−6859.

(74) Horne, W. J.; Andrews, M. A.; Terrill, K. L.; Hayward, S. S.; Marshall, J.; Belmore, K. A.; Shannon, M. S.; Bara, J. E. Poly(Ionic Liquid) Superabsorbent for Polar Organic Solvents. *ACS Appl. Mater. Interfaces* **2015**, *7*, 8979−8983.

(75) Wang, B.; Feng, Y.; Qi, X.; Deng, M.; Tian, J.; Zhang, Q. Designing Explosive Poly(Ionic Liquid)s as Novel Energetic Polymers. *Chem. - Eur. J.* **2018**, *24*, 15897−15902.

(76) Zertal, Y.; Yong, M.; Levi, A.; Sevilia, S.; Tsoglin, A.; Parvari, G.; Gottlieb, L.; Eichen, Y. Alkyl Vinyl Imidazolium Ionic Liquids as Fuel Binders for Photo-curable Energetic Propellants. *ACS Appl. Polym. Mater.* **2022**, *4*, 4928−4939.

(77) Hsu, C.-H.; Kuo, S.-W.; Chen, J.-K.; Ko, F.-H.; Liao, C.-S.; Chang, F.-C. Self-Assembly Behavior of A-B Diblock and C-D Random Copolymer Mixtures in the Solution State through Mediated Hydrogen Bonding. *Langmuir* **2008**, *24*, 7727−7734.

(78) Kuo, S.-W. Hydrogen bond-mediated self-assembly and supramolecular structures of diblock copolymer mixtures. *Polym. Int.* **2009**, *58*, 455−464.

(79) Horkay, F. Polyelectrolyte Gels: A Unique Class of Soft Materials. *Gels* **2021**, *7*, 102.

(80) Muthukumar, M. 50th Anniversary Perspective: A Perspective on Polyelectrolyte Solutions. *Macromolecules* **2017**, *50*, 9528−9560.

(81) Wanasingha, N.; Dorishetty, P.; Dutta, N. K.; Choudhury, N. R. Polyelectrolyte Gels: Fundamentals, Fabrication and Applications. *Gels* **2021**, *7*, 148.

(82) Elias, H.-G. *An Introduction to Polymer Science*; Wiley, 1997.

(83) Borisov, O. V.; Zhulina, E. B. Effect of Salt on Self-Assembly in Charged Block Copolymer Micelles. *Macromolecules* **2002**, *35*, 4472−4480.

(84) Chavan, S. N.; Lee, H.-i. Random ionic polymers: Salt-triggered reversible vesicular self-assembly in water. *Eur. Polym. J.* **2023**, *193*, No. 112114.

(85) Isik, M.; Fernandes, A. M.; Vijayakrishna, K.; Paulis, M.; Mecerreyes, D. Preparation of poly(ionic liquid) nanoparticles and their novel application as flocculants for water purification. *Polym. Chem.* **2016**, *7*, 1668−1674.

(86) Korchagina, E. V.; Philippova, O. E. Ion-Specific Self-Assembly of Hydrophobically Modified Polycation of Natural Origin. *Macromolecules* **2015**, *48*, 8622−8628.

(87) Popescu, M.-T.; Liontos, G.; Avgeropoulos, A.; Tsitsilianis, C. Stimuli responsive fibrous hydrogels from hierarchical self-assembly of a triblock copolypeptide. *Soft Matter* **2015**, *11*, 331−342.

(88) Zhong, J.; Luo, H.; Tang, Q.; Lei, Z.; Tong, Z. Counterion-Mediated Self-Assembly of Ion-Containing Block Copolymers on the

Basis of the Hofmeister Series. *Macromol. Chem. Phys.* **2019**, *220*, No. 1800554.

(89) Dazzi, A.; Prater, C. B. AFM-IR: Technology and Applications in Nanoscale Infrared Spectroscopy and Chemical Imaging. *Chem. Rev.* **2017**, *117*, 5146−5173.

(90) Mathurin, J.; Deniset-Besseau, A.; Bazin, D.; Dartois, E.; Wagner, M.; Dazzi, A. Photothermal AFM-IR spectroscopy and imaging: Status, challenges, and trends. *J. Appl. Phys.* **2022**, *131*, No. 010901.

(91) Tseng, Y.-H.; Fan, Y.-C.; Chang, C.-T.; Lin, Y.-L.; Chang, C.-W.; Liao, C.-W.; Chen, J.-T. Photoinduced Alignment under Solvent Vapor Annealing (PA-SVA): Enhanced Ordering and Patterning in Block Copolymer Films. *ACS Appl. Polym. Mater.* **2022**, *4*, 8536−8542.

(92) Ramer, G.; Ruggeri, F. S.; Levin, A.; Knowles, T. P. J.; Centrone, A. Determination of Polypeptide Conformation with Nanoscale Resolution in Water. *ACS Nano* **2018**, *12*, 6612−6619.

(93) Ruggeri, F. S.; Habchi, J.; Chia, S.; Horne, R. I.; Vendruscolo, M.; Knowles, T. P. J. Infrared nanospectroscopy reveals the molecular interaction fingerprint of an aggregation inhibitor with single Aβ42 oligomers. *Nat. Commun.* **2021**, *12*, No. 688.

(94) da Silva, P. M. M.; Camparotto, N. G.; Figueiredo Neves, T.; Mastelaro, V. R.; Nunes, B.; Siqueira Franco Picone, C.; Prediger, P. Instantaneous adsorption and synergic effect in simultaneous removal of complex dyes through nanocellulose/graphene oxide nano-composites: Batch, fixed-bed experiments and mechanism. *Environ. Nanotechnol., Monit. Manage.* **2021**, *16*, No. 100584.

(95) Nguyen-Tri, P.; Nguyen, V. T.; Nguyen, T. A. Biological Activity and Nanostructuration of Fe3O4-Ag/High Density Poly-ethylene Nanocomposites. *J. Compos. Sci.* **2019**, *3*, 34.

(96) Li, H.; Buesen, D.; Williams, R.; Henig, J.; Stapf, S.; Mukherjee, K.; Freier, E.; Lubitz, W.; Winkler, M.; Happe, T.; Plumeré, N. Preventing the coffee-ring effect and aggregate sedimentation by in situ gelation of monodisperse materials. *Chem. Sci.* **2018**, *9*, 7596−7605.

(97) Kaliyaraj Selva Kumar, A.; Zhang, Y.; Li, D.; Compton, R. G. A mini-review: How reliable is the drop casting technique? *Electrochem. Commun.* **2020**, *121*, No. 106867.

(98) Schwartz, J. J.; Jakob, D. S.; Centrone, A. A guide to nanoscale IR spectroscopy: resonance enhanced transduction in contact and tapping mode AFM-IR. *Chem. Soc. Rev.* **2022**, *51*, 5248−5267.

(99) Albert, J. N. L.; Epps, T. H. Self-assembly of block copolymer thin films. *Mater. Today* **2010**, *13*, 24−33.

(100) Kim, H.-C.; Hinsberg, W. D. Surface patterns from block copolymer self-assembly. *J. Vac. Sci. Technol., A* **2008**, *26*, 1369−1382.

(101) Steinert, M.; Acker, J.; Oswald, S.; Wetzig, K. Study on the Mechanism of Silicon Etching in HNO3-Rich HF/HNO3 Mixtures. *J. Phys. Chem. C* **2007**, *111*, 2133−2140.

(102) Almeida, R. M.; Guiton, T. A.; Pantano, C. G. Character-ization of silica gels by infrared reflection spectroscopy. *J. Non-Cryst. Solids* **1990**, *121*, 193−197.

(103) Osswald, J.; Fehr, K. T. FTIR spectroscopic study on liquid silica solutions and nanoscale particle size determination. *J. Mater. Sci.* **2006**, *41*, 1335−1339.

(104) De Cupere, V. M.; Gohy, J. F.; Jérome, R.; Rouxhet, P. G. Influence of substrate hydrophobicity on the adsorption of an amphiphilic diblock copolymer. *J. Colloid Interface Sci.* **2004**, *271*, 60−68.

(105) Cummins, C.; Lundy, R.; Walsh, J. J.; Ponsinet, V.; Fleury, G.; Morris, M. A. Enabling future nanomanufacturing through block copolymer self-assembly: A review. *Nano Today* **2020**, *35*, No. 100936.

(106) Majewski, P. W.; Yager, K. G. Rapid ordering of block copolymer thin films. *J. Phys.: Condens. Matter* **2016**, *28*, No. 403002.